

$N^3\text{LO}+N^3\text{LL}$ QCD improved Higgs pair cross sections

A.H. Ajjath and Hua-Sheng Shao

Laboratoire de Physique Théorique et Hautes Energies (LPTHE), UMR 7589, Sorbonne Université et CNRS, 4 place Jussieu, 75252 Paris Cedex 05, France

E-mail: aabdulhameed@lpthe.jussieu.fr, huasheng.shao@lpthe.jussieu.fr

ABSTRACT: We report a new calculation of the soft-gluon threshold resummation for the Higgs boson pair production in the dominant production mode – gluon-gluon fusion – up to the next-to-next-to-next-to-leading logarithmic ($N^3\text{LL}$) accuracy. After matching $N^3\text{LL}$ to the next-to-next-to-next-to-leading order ($N^3\text{LO}$) QCD calculation in the infinite top quark mass approximation, we show that the central values of the inclusive cross sections are quite stable with respect to $N^3\text{LO}$, while the conventional renormalisation and factorisation scale uncertainties are reduced by a factor of two, reaching to the subpercent level. Our study further consolidates the good asymptotic perturbative convergence. After combining with the full top-quark mass dependent next-to-leading order QCD results, our most advanced predictions are presented for both the inclusive total cross sections and the differential invariant mass distributions of the Higgs pair.

KEYWORDS: Higgs, QCD, LHC

Contents

1	Introduction	1
2	Theoretical framework	5
2.1	General structure	5
2.2	Soft-virtual limit	6
2.3	Threshold resummation	11
2.4	Ambiguities in resummation and resummation schemes	15
2.5	N ³ LL resummation for Higgs boson pair production	17
3	Results	19
3.1	Impact of QCD corrections in the infinite top quark mass approximation	19
3.2	N ³ LO+N ³ LL improved cross sections with full top-quark mass dependence	23
4	Summary	28
A	The universal N³LL resummed coefficients	29

1 Introduction

The studies of the 125 GeV Higgs boson h at the Large Hadron Collider (LHC) turn into the second decade since its discovery [1, 2]. Many Higgs properties, such as its mass, width, spin and CP, have been thoroughly investigated. Its interactions with the force carriers (Z, W, γ , and gluon g) and the third-generation charged fermions (t, b, τ) have all been established, which are compatible with the Standard Model (SM) predictions within $\sim 10\%$ accuracy [3, 4]¹. The observation of the Yukawa coupling between the Higgs boson and the first second-generation fermion muon is in reach. One of the central questions remaining to be answered at the LHC is that whether the Higgs boson interacts with itself. A remarkable prediction of the SM is that, analogous to the way of Higgs boson interacting with other massive elementary particles, the self-interaction strength of the Higgs boson scales with its mass. The latter has been measured to be around 0.1 to 0.2% accuracy. The knowledge of the Higgs self interactions is essential to scrutinize the Higgs field potential, a key to understand the electroweak spontaneous symmetry breaking mechanism and on how the subatomic particles acquire their masses. The only thing we know about the potential so far is from the mass m_h of the Higgs boson, which is the second derivative of the potential with respect to the Higgs field around the (local) minimum of potential, at which the Higgs field averagely takes the non-zero vacuum expectation value $v \approx 246.2$ GeV.

¹A caveat: the quoted uncertainties may vary depending on the assumptions that have been made.

The shape of the Higgs potential has in fact the far reaching influences on cosmology (see e.g., refs. [5, 6]). The distinct fates of our universe are determined by the vacuum stability or instability of the potential. In the former case, the current minimum at $v \approx 246.2$ GeV is the global minimum, while it is just a local minimum in the latter case. Thus, our universe will decay through quantum tunnelling at some point in the future if the vacuum is unstable [7]. This is the case predicted in the SM [8–11]. Such an instability can be cured in many beyond the SM (BSM) theories. The role of the Higgs field is also crucial in the early universe. In particular, at around a nanosecond after the big bang, the universe underwent from the electroweak symmetry unbroken phase to the broken phase [12]. Such a phase transition could be a first or second order as well as a crossover depending on the Higgs potential. Lattice calculations [13, 14] show that it should be a crossover in the setup of the SM. The (strong) first-order phase transition provides one necessary condition [15] for generating matter-antimatter asymmetry at the electroweak scale. Besides, the first-order transition may leave a few detectable cosmic imprints, such as primordial ² gravitational waves [16, 17] and magnetic fields [18], and topological defects.

As aforementioned, the crucial input to pin down the Higgs potential is by measuring the Higgs self interactions. These self interactions are accessible by studying the multiple-Higgs boson production from high-energy particle collisions, such as at the LHC [19] or the future colliders [20, 21]. The most viable production mode is the production of a pair of Higgs bosons. We will concentrate on the process of the Higgs boson pair production at hadron colliders in this paper. Such a process is vital in directly probing the Higgs trilinear self coupling λ_{hhh} [22] and in indirectly constraining the Higgs quartic self coupling [23, 24], where in the SM λ_{hhh} is uniquely fixed by the Higgs mass and the vacuum expectation value via $\lambda_{hhh}^{\text{SM}} = \frac{m_h^2}{2v^2} \approx 0.129$. Due to the pattern of the couplings between the Higgs boson and other SM particles, Higgs boson is very hard to be experimentally detected (partially) because of its low production rates and the small branching fractions of the background-clean decay modes. The di-Higgs is more than doubling the challenges. The di-Higgs production cross sections are three orders of magnitude smaller than the single Higgs counterparts, in which the two Higgs bosons are predominantly produced in the fusions of two initial gluons emitted by protons (see figure 1).

The paper will focus on quantifying the high precision Higgs pair production cross sections via the gluon-gluon fusion (ggF) channel. We want to stress that the target precision is strongly tied to determine how large portion of the BSM scenarios can be probed (cf., e.g., figure 1 in ref. [25]). A question of “if we measure a deviation of the trilinear Higgs coupling with respect to the SM value $\delta_\lambda \equiv \kappa_\lambda - 1 \equiv \frac{\lambda_{hhh}}{\lambda_{hhh}^{\text{SM}}} - 1 \neq 0$, what is the energy scale that the new physics lies ?” is pursued in refs. [26, 27]. For instance, ref. [27] finds the perturbation theory breaks at the scale $\lesssim \frac{13 \text{ TeV}}{|\delta_\lambda|}$ regardless of the shape of the Higgs potential. It means that a BSM dynamics should exist in the 130 TeV (1.3 PeV) regime with a 10% (1%) deviation of $|\delta_\lambda|$ from 0. Therefore, the capability of identifying a small BSM signature requires us to improve the theoretical systematic control in the SM.

²The word “primordial” here means that the gravitational waves and magnetic fields are not produced by the astronomical objects. They are really leftovers from the cosmic evolution.

The existing direct measurements of the Higgs boson pair cross sections at the LHC only loosely bound on the trilinear Higgs self-coupling λ_{hhh} so far. The current best constraints $-1.24 < \kappa_\lambda < 6.49$ and $-0.6 < \kappa_\lambda < 6.6$ at 95% confidence level were placed by the CMS [4] and ATLAS [28] collaborations respectively.³ Although the results are very encouraging, the limit does not yet reach to most of the interesting regions of the vast BSM scenarios (see, e.g., refs. [29–33]). It is even just touching the range $|\delta_\lambda| = |\kappa_\lambda - 1| < 5$ set by the perturbativity argument [34]. The precision of κ_λ will be largely improved at the HL-LHC with 3000 fb^{-1} integrated luminosity [20] and the envisaged future hadron colliders [21, 35, 36]. δ_λ is estimated to be achievable better than $\pm 50\%$ (around $\pm 5\%$) at the HL-LHC (a future 100 TeV pp collider).⁴

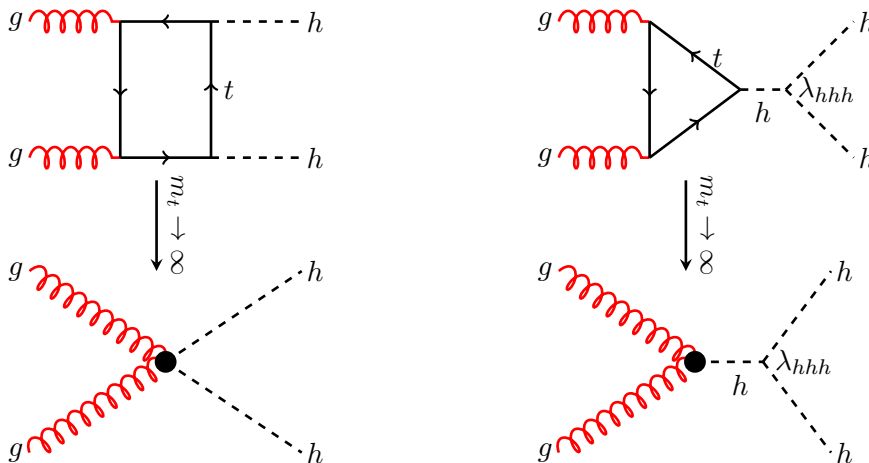


Figure 1: Representative lowest order Feynman diagrams of $gg \rightarrow hh$ in the SM with full top quark mass dependence (upper) and in the heavy/infinite top quark mass approximation (lower).

Before moving on, we briefly describe how the cross sections of the ggF process $gg \rightarrow hh$ are calculated in the SM. The perturbative calculations for the process are quite challenging due to the absence of the tree-level interactions between the Higgs boson and the gluon. The leading order (LO) cross section is derived from the square of the one-loop amplitude dominantly via the virtual top quark loop, where two representative Feynman diagrams can be found in the upper row of figure 1. The higher-order QCD perturbative calculations are very difficult due to the complicated multi-loop multi-scale Feynman integrals. Thanks to the new technology development of the numerical approaches [37–39], the next-to-leading order (NLO) results are presented in refs. [40–45]. The NLO calculation has been further

³In ATLAS paper [28], the best constraint by combining the Higgs pair cross section and the loop effects from the single Higgs process is $-0.4 < \kappa_\lambda < 6.3$. The electroweak loop effects from the single Higgs production can indirectly probe λ_{hhh} . However at the HL-LHC, the indirect limit would be harder to be improved since it is dominated by the systematic errors.

⁴There is, however, a caveat in order to interpret these numbers. The values of δ_λ were derived based on several assumptions extrapolated from what have been understood or used in the LHC Run 2 analysis, where the theoretical uncertainties have been assumed to be reduced by a factor of two with respect to the state of the art at the time.

improved either by soft-gluon resummation [46, 47] or after matching to parton showers [48–50]. These are the best results achieved so far by taking into account the full top quark mass m_t dependence. They leave a few theory challenges to be tackled in the future. First of all, the NLO results are plagued with the large theoretical uncertainties both from the scale variations [40] and the top-quark mass scheme dependence [42]. Some differential distributions may differ significantly by adopting different matching schemes [48] or using different shower scales [49].

A second useful way of improving the cross sections is applying the so-called infinite top quark mass approximation,⁵ denoting as $m_t \rightarrow \infty$. In such an approximation, the top quark loops shrink to the contact points (cf. the bullets in the lower row of figure 1) by taking the heavy top quark mass approximation $m_t \gg m_h$ in the amplitude. Under this working approximation, we have circumvented the aforementioned complicated multi-loop Feynman integrals. One is therefore able to go beyond much further than the loop-induced case, albeit still with a lot of theoretical efforts needed. The state-of-the-art perturbative QCD calculation in the $m_t \rightarrow \infty$ approximation is next-to-next-to-next-to-leading order (N³LO) [51, 52], which was certainly impossible without the decades of theoretical efforts [53–72] by the whole community. Although N³LO QCD corrections only enhance the central values of next-to-next-to-leading order (NNLO) by 3%, the renormalisation and factorisation scale uncertainties are dramatically reduced by a factor of 3 to 4 to reach to the percent level accuracy. The soft-gluon resummation effects have been studied up to NNLO plus next-to-next-to-leading logarithmic (NNLL) accuracy in ref. [73].⁶ The finite top quark mass corrections can be included either by taking into account more terms in the $\frac{m_h^2}{m_t^2}$ expansion [43, 75–79] or by rescaling $m_t \rightarrow \infty$ amplitudes (cross sections) with the known full- m_t dependent amplitudes (cross sections) [52, 80–82]. Moreover, there are also many interesting attempts to compute the two-loop ggF di-Higgs amplitudes in the analytic forms by taking various approximations [83–87]. Recently, partial results of the NLO electroweak corrections, namely from the top Yukawa coupling induced, become available [88, 89].

In this work, we further improve the perturbative QCD calculations of $gg \rightarrow hh$ with the threshold resummation up to next-to-next-to-next-to-leading logarithmic (N³LL) accuracy in the infinite top quark mass approximation. We discuss the theoretical uncertainties that are stemming from the ambiguities in resummation. The final results, ready for phenomenological applications, are reported as N³LL matched to N³LO (N³LO+N³LL), which are also augmented with the known full m_t -dependent NLO calculation.

The remainder of the paper is organised as follows. We describe our theoretical framework in section 2. Our results are reported in section 3. The conclusions are drawn in section 4. The concrete expressions of the universal coefficients appearing in the N³LL resummation for $gg \rightarrow hh$ can be found in appendix A.

⁵It is also alternatively called the “heavy top quark mass approximation” or “large top quark mass approximation” or dubbed as the Higgs effective field theory (HEFT) approach in the literature.

⁶An earlier threshold resummation at a lower accuracy was carried out in ref. [74].

2 Theoretical framework

2.1 General structure

For a general hadronic process with hadrons h_1 and h_2 collide to produce a heavy colourless final state with the invariant mass square M^2 , the differential invariant mass distribution in QCD improved parton model takes the form of a convoluted integral:

$$M^2 \frac{d}{dM^2} \sigma_{h_1 h_2}(s, M^2) = \tau \sum_{a,b=q,\bar{q},g} \int_{\tau}^1 \frac{dz}{z} \phi_{ab} \left(\frac{\tau}{z}, \mu_F^2 \right) \Delta_{ab}(z, M^2, \mu_F^2). \quad (2.1)$$

Here, s is the square of the hadronic center-of-mass energy, μ_F is the factorisation scale and the dimensionless quantity τ is defined as $\tau \equiv \frac{M^2}{s}$. The partonic luminosity ϕ_{ab} is defined as the convolution of parton distribution functions (PDFs) f_{a/h_1} and f_{b/h_2} :

$$\phi_{ab}(x, \mu_F^2) \equiv \int_x^1 \frac{dy}{y} f_{a/h_1}(y, \mu_F^2) f_{b/h_2} \left(\frac{x}{y}, \mu_F^2 \right). \quad (2.2)$$

While the partonic coefficient function Δ_{ab} is perturbatively calculable in QCD, and is expanded in terms of $a_s \equiv \alpha_s/(4\pi)$ with α_s being the UV renormalised strong coupling constant. In the collinear factorisation, the partonic coefficient function is expressed in terms of the bare partonic cross section $\hat{\sigma}_{ab}$ and the splitting kernels Γ at the scale μ_F :

$$\Delta_{ab}(z, M^2, \mu_F^2) = \sum_{c,d} \Gamma_{ca}^{-1}(z, \mu_F^2, \mu^2, \epsilon) \otimes \frac{1}{z} \hat{\sigma}_{cd}(z, M^2, \mu^2, \epsilon) \otimes \Gamma_{db}^{-1}(z, \mu_F^2, \mu^2, \epsilon), \quad (2.3)$$

with all the initial collinear singularities encapsulated in Γ , in terms of the regularised Altarelli-Parisi (AP) splitting functions⁷. The μ_F dependence, in principle, should cancel order by order at the hadronic level after convoluting $\Delta_{ab}(z, M^2, \mu_F^2)$ with the partonic luminosity. μ in eq. (2.3) is the regularisation scale in the dimensional regularisation with $d = 4 - 2\epsilon$ spacetime dimensions. The symbol \otimes refers to the convolution operator defined for arbitrary functions $f_i(x), i = 1, 2, \dots, n$ as:

$$f_1(z) \otimes f_2(z) \otimes \dots \otimes f_n(z) \equiv \prod_{i=1}^n \left(\int_0^1 dx_i f_i(x_i) \right) \delta(z - x_1 x_2 \dots x_n). \quad (2.4)$$

The bare partonic cross section $\hat{\sigma}_{ab}$ can be expanded in $\hat{a}_s \equiv \frac{\hat{\alpha}_s}{4\pi}$ with the bare strong coupling constant $\hat{\alpha}_s$:

$$\hat{\sigma}_{ab}(z, M^2, \mu^2, \epsilon) = \hat{a}_s^b S_\epsilon^b \left[\hat{\sigma}_{ab}^{(0)} \delta(1-z) + \sum_{k=1} \hat{a}_s^k \hat{\sigma}_{ab}^{(k)} \right], \quad (2.5)$$

where b is the power of \hat{a}_s at the lowest order and $S_\epsilon \equiv (4\pi e^{-\gamma_E})^\epsilon$ in the spacetime dimension $d = 4 - 2\epsilon$ with γ_E being the Euler-Mascheroni constant. Beyond the lowest order in \hat{a}_s , the coefficient $\hat{\sigma}_{ab}^{(k)}$ involves UV and IR divergences. The UV renormalisation

⁷The lowest order is $\Gamma_{ab}^{-1} = \delta_{ab}$ where δ_{ab} is the Kronecker delta function.

procedure removes the UV singularities and introduces a dependence on the renormalisation scale μ_R . In the $\overline{\text{MS}}$ scheme, the renormalised coupling constant a_s is related to the bare coupling \hat{a}_s via

$$\hat{a}_s S_\epsilon = \left(\frac{\mu^2}{\mu_R^2} \right)^{-\epsilon} Z_{\alpha_s}(\mu_R^2) a_s(\mu_R^2), \quad (2.6)$$

which satisfies the renormalisation group running $\frac{d}{d \ln \mu_R^2} a_s = \beta(a_s) - \epsilon a_s$ in $d = 4 - 2\epsilon$ dimensions. The beta function ensures the following series expansion

$$\beta(a_s) = -a_s \sum_{k=0} \beta_k a_s^{k+1} \quad (2.7)$$

with $\beta_0 = \frac{11}{3}C_A - \frac{4}{3}T_F n_q$, $\beta_1 = \frac{1}{3}(34C_A^2 - 12C_F T_F n_q - 20C_A T_F n_q)$, etc. Here, $C_F = \frac{4}{3}$ and $C_A = 3$ are Casimir constants, $T_F = \frac{1}{2}$ and n_q is the number of massless quark flavours. The renormalisation group invariance of the bare coupling constant $\frac{d}{d \ln \mu_R^2} \ln \hat{a}_s = 0$ gives us $\beta(a_s(\mu_R^2)) = -a_s(\mu_R^2) \frac{d}{d \ln \mu_R^2} \ln Z_{\alpha_s}(\mu_R^2)$ with

$$\begin{aligned} Z_{\alpha_s}(\mu_R^2) = & 1 + a_s(\mu_R^2) \left[-\frac{\beta_0}{\epsilon} \right] + a_s^2(\mu_R^2) \left[\frac{\beta_0^2}{\epsilon^2} - \frac{\beta_1}{2\epsilon} \right] + a_s^3(\mu_R^2) \left[-\frac{\beta_0^3}{\epsilon^3} + \frac{7}{6\epsilon^2} \beta_0 \beta_1 - \frac{\beta_2}{3\epsilon} \right] \\ & + a_s^4(\mu_R^2) \left[\frac{\beta_0^4}{\epsilon^4} - \frac{23}{12\epsilon^3} \beta_0^2 \beta_1 + \frac{1}{\epsilon^2} \left(\frac{3}{8} \beta_1^2 + \frac{5}{6} \beta_0 \beta_2 \right) - \frac{1}{4\epsilon} \beta_3 \right] + \mathcal{O}(a_s^5). \end{aligned} \quad (2.8)$$

If the amplitude depends on other bare couplings like the Higgs Yukawa couplings or the other effective couplings, it is understood that the similar UV renormalisation should be carried out. For simplicity, we ignore the dependence on other couplings in the following context.

The α_s series expansion given in eq.(2.5) is usually referring as the fixed order perturbative calculations. However, the perturbative expansion has limitations in its applicability if the coefficients at each order involve large logarithms. Such cases could arise from the soft-gluon emissions. Despite the cancellation of soft singularities between virtual and real radiative contributions, soft gluon effects can yield potentially large logarithms in the kinematic configurations where high imbalance between real and virtual gluons happens. In such cases, the threshold resummation is suitable to be performed by resumming these large logarithms to all orders in α_s , which is exactly the subject of the present paper.

2.2 Soft-virtual limit

Let us define the threshold limit in terms of the partonic variable $z \equiv \frac{M^2}{\hat{s}} \rightarrow 1$, with \hat{s} being the square of the partonic center of mass energy. As the name implies, in this phase space region, almost all the incoming partonic center of mass energy goes to produce the Born-like final state, and the residual energy is only sufficient to generate soft gluons.

In this limit, the partonic coefficient function can be organised into two parts:

$$\Delta_{ab}(z, M^2, \mu_F^2) = \Delta_{ab}^{\text{SV}}(z, M^2, \mu_F^2) + \Delta_{ab}^{\text{Reg}}(z, M^2, \mu_F^2). \quad (2.9)$$

In such a decomposition, the term $\Delta_{ab}^{\text{SV}}(z, M^2, \mu_F^2)$ involves only the singular terms when $z = 1$ with the distributions of the following forms:

$$\left\{ \delta(1-z), \mathcal{D}_i(z) \equiv \left[\frac{\ln^i(1-z)}{1-z} \right]_+ \right\}, \quad (2.10)$$

where $\delta(1-z)$ is the Dirac delta function and $\mathcal{D}_i(z)$ is a plus distribution. The latter is defined as that for any test function $f(z)$, there is

$$\int_0^1 dz \mathcal{D}_i(z) f(z) = \int_0^1 dz \frac{\ln^i(1-z)}{1-z} [f(z) - f(1)]. \quad (2.11)$$

The superscript SV denotes the soft-virtual part, accounting for the real emission corrections at the threshold limit and the pure virtual corrections. The remaining regular term $\Delta_{ab}^{\text{Reg}}(z, M^2, \mu_F^2)$ contains either $\ln^i(1-z)$ terms or the polynomials of $(1-z)$. Although the logarithms $\ln^i(1-z)$ could also be large, they are subdominant by a factor of $(1-z)$ compared to the soft-virtual contribution. In the following discussion, we ignore these subleading power terms.

Since we focus on soft-virtual part in the context, only the flavour diagonal terms of Γ in eq.(2.3) contribute. Hence, the parton flavour sum in eq.(2.3) can be safely omitted, giving rise to a simpler relation:

$$\Delta_{ab}^{\text{SV}}(z, M^2, \mu_F^2) = \Gamma_{aa}^{-1}(z, \mu_F^2, \mu^2, \epsilon) \otimes \frac{1}{z} \hat{\sigma}_{ab}^{\text{SV}}(z, M^2, \mu^2, \epsilon) \otimes \Gamma_{bb}^{-1}(z, \mu_F^2, \mu^2, \epsilon). \quad (2.12)$$

Again, the superscript SV indicates that we only keep those terms which give rise to $\delta(1-z)$ and \mathcal{D}_i . The soft-virtual partonic cross section can be further factorised into the soft and hard (or virtual) parts. In this respect, the partonic coefficient function further takes the form:

$$\begin{aligned} \Delta_{ab}^{\text{SV}}(z, M^2, \mu_F^2) &= \hat{a}_s^b S_\epsilon^b \hat{\sigma}_{ab}^{(0)} |\mathcal{F}_{ab}(M^2, \mu^2, \epsilon)|^2 \delta(1-z) \otimes \\ &(\mathcal{S}_{ab}(z, M^2, \mu^2, \epsilon) \otimes \Gamma_{aa}^{-1}(z, \mu_F^2, \mu^2, \epsilon) \otimes \Gamma_{bb}^{-1}(z, \mu_F^2, \mu^2, \epsilon)). \end{aligned} \quad (2.13)$$

The form factor \mathcal{F}_{ab} captures pure loop corrections and starts from 1 as the lowest term. The implicit dependence of the form factor on external particle momenta, colours and spins is left understood. The soft function \mathcal{S}_{ab} embeds the real soft-gluon corrections. Each piece on the right-hand side of eq. (2.13) is not UV renormalised yet. Hence they involve UV divergences, which should be removed by the UV renormalisation. \mathcal{F}_{ab} and \mathcal{S}_{ab} contain IR poles as well. Δ_{ab}^{SV} , on the other hand, is both UV and IR finite, the details of which will be discussed shortly.

In dimensional regularisation, the IR divergences in the form factor stemming from the soft and collinear loop-momentum modes can be renormalised as ⁸:

$$\hat{a}_s^b S_\epsilon^b \hat{\sigma}_{ab}^{(0)} |\mathcal{F}_{ab}(M^2, \mu^2, \epsilon)|^2 = \lim_{\epsilon \rightarrow 0} |Z_{ab}^{\text{IR}}(M^2, \mu_R^2, \epsilon)|^2 H_{ab}(M^2, \mu_R^2). \quad (2.14)$$

⁸In the following, if an object has the dependence on the renormalisation scale μ_R , it means we have carried out the UV renormalisation for the coupling constant α_s unless we explicitly write out its dependence on \hat{a}_s or $\hat{\alpha}_s$. After the UV renormalisation, there is no explicit μ dependence anymore, because the regularisation scale in the dimensional regularisation is always in the form of $(\mu^2)^\epsilon$ for each loop-momentum integration.

A few comments are in order. The coupling constant is renormalised on the right-hand side. Both Z_{ab}^{IR} and H_{ab} are perturbatively expanded in terms of the renormalised coupling constant a_s . Z_{ab}^{IR} factorises all the IR divergences coming from the virtual amplitudes. The hard function H_{ab} is finite and depends on the Born kinematics, such that the lowest order equals to the Born amplitude squared. From the IR factorisation of virtual amplitudes, it is well-known that Z_{ab}^{IR} is a universal quantity [90–99]. For colourless particles production, it is insensitive to the hard process under study and only depends on if the process is initial quark or gluon induced. More specifically, the IR singularities of the virtual contribution are solely determined by the nature of the initial particles. This in turn leads to the fact that the combined contributions from the soft function \mathcal{S}_{ab} and the kernels Γ^{-1} must exhibit the same universal IR divergences. Absorbing Z_{ab}^{IR} into the second line of eq.(2.13) and performing the coupling constant renormalisation at the scale μ_R yields:

$$\Delta_{ab}^{\text{SV}}(z, M^2, \mu_F^2) = H_{ab}(M^2, \mu_R^2) \delta(1-z) \otimes S_{\Gamma,ab}(z, M^2, \mu_F^2, \mu_R^2) \quad (2.15)$$

with

$$S_{\Gamma,ab}(z, M^2, \mu_F^2, \mu_R^2) \equiv \lim_{\epsilon \rightarrow 0} |Z_{ab}^{\text{IR}}(M^2, \mu_R^2, \epsilon)|^2 \delta(1-z) \otimes [\mathcal{S}_{ab}(z, M^2, \mu_R^2, \epsilon) \otimes \Gamma_{aa}^{-1}(z, \mu_F^2, \mu_R^2, \epsilon) \otimes \Gamma_{bb}^{-1}(z, \mu_F^2, \mu_R^2, \epsilon)] . \quad (2.16)$$

Since the IR divergent part of $(\mathcal{S}_{ab} \otimes \Gamma_{aa}^{-1} \otimes \Gamma_{bb}^{-1})$ cancels against $|Z_{ab}^{\text{IR}}|^2$, both H_{ab} and $S_{\Gamma,ab}$ are free of IR poles. The hard function H_{ab} is obtained from the IR subtracted loop corrections⁹. On the other hand, the structure of soft-collinear part $S_{\Gamma,ab}$ is obtained by computing real corrections and the AP splitting kernels in the soft limit. Alternatively, one can also predict the structure of soft-collinear part $S_{\Gamma,ab}$ by employing its universal behaviour. This leads to a framework to resum the large logarithms present at the threshold limit, which we discuss briefly in the following.

We begin with the ingredients in eq.(2.13). The structure of splitting kernel Γ_{aa} is well-known. It satisfies the renormalisation group evolution equation with respect to μ_F :

$$\mu_F^2 \frac{d}{d\mu_F^2} \Gamma_{aa}(z, \mu_F^2, \mu_R^2, \epsilon) = \frac{1}{2} P_{aa}(z, a_s(\mu_F^2)) \otimes \Gamma_{aa}(z, \mu_F^2, \mu_R^2, \epsilon) + \mathcal{O}(1), \quad (2.17)$$

where P_{aa} is the regularised flavour diagonal (unpolarised) AP splitting function¹⁰. Note here that in the above equation, we have dropped the contributions from off-diagonal splitting functions since we focus on the soft-virtual contributions only. The diagonal splitting function at the production threshold takes the form:

$$P_{aa}(z, a_s(\mu_F^2)) = 2B_a(a_s(\mu_F^2))\delta(1-z) + 2A_a(a_s(\mu_F^2))\mathcal{D}_0(z) + \mathcal{O}(1), \quad (2.18)$$

⁹Both H_{ab} and $S_{\Gamma,ab}$ are IR subtraction scheme dependent due to the ambiguities in choosing Z_{ab}^{IR} . However, the combination of the two, Δ_{ab}^{SV} , is independent of the subtraction scheme.

¹⁰The three-loop unpolarised AP splitting functions are known in refs. [100, 101]. The non-singlet ones have been checked in ref. [102] with a different approach.

in terms of the light-like cusp A_a ¹¹ and the virtual B_a ¹² anomalous dimensions, which depend only on the nature of incoming particle a . In particular, we notice that $A_a(a_s) = \sum_{k=1} a_s^k A_a^{(k)} = a_s 4C_a + \mathcal{O}(a_s^2)$ and $B_a(a_s) = \sum_{k=1} a_s^k B_a^{(k)} = \begin{cases} a_s \beta_0 + \mathcal{O}(a_s^2), & a = g \\ a_s 3C_F + \mathcal{O}(a_s^2), & a = q, \bar{q} \end{cases}$, where $C_q = C_{\bar{q}} = C_F$ and $C_g = C_A$ are Casimir constants. The solution of eq. (2.17) is found to be

$$\Gamma_{aa}(z, \mu_F^2, \mu^2, \epsilon) = \delta(1-z) + \sum_{k=1} \hat{a}_s^k S_\epsilon^k \left(\frac{\mu_F^2}{\mu^2} \right)^{-k\epsilon} \Gamma_{aa}^{(k)}(z, \epsilon). \quad (2.19)$$

The expressions of $\Gamma_{aa}^{(k)}(z, \epsilon)$ up to $k = 4$ in the $\overline{\text{MS}}$ scheme can be found in eq. (33) of ref. [107] by replacing ϵ with -2ϵ . In particular, $\Gamma_{aa}^{(1)}(z, \epsilon) = -\frac{1}{\epsilon} \left(A_a^{(1)} \mathcal{D}_0(z) + B_a^{(1)} \delta(1-z) + \mathcal{O}(1) \right)$.

The structure of the soft function \mathcal{S}_{ab} could be determined from the behaviour of the Sudakov form factor through its evolution under the momentum transfer M^2 , which leads to its exponentiation [108–110], and the renormalisation group evolution of the splitting kernels Γ_{aa} and Γ_{bb} . The universal factorisation of IR singularities guarantees that the soft function could be expressed in terms of a first order differential equation. From eq.(2.13), we can derive

$$\begin{aligned} M^2 \frac{d}{dM^2} \ln \mathcal{S}_{ab} &= M^2 \frac{d}{dM^2} \ln \Delta_{ab}^{SV} - M^2 \frac{d}{dM^2} \left(2 \ln \mathcal{F}_{ab} + \ln \hat{\sigma}_{ab}^{(0)} \right) \delta(1-z) \\ &= -2M^2 \frac{d}{dM^2} \ln Z_{ab}^{\text{IR}} \delta(1-z) + M^2 \frac{d}{dM^2} \ln S_{\Gamma, ab} \\ &= -2M^2 \frac{d}{dM^2} \ln Z_{ab}^{\text{IR}} \delta(1-z) + M^2 \frac{d}{dM^2} \ln S_{ab}^{\text{fin}} \\ &= \overline{K}_{ab} \left(\hat{a}_s, \frac{\mu_R^2}{\mu^2}, z, \epsilon \right) + \overline{G}_{ab} \left(\hat{a}_s, \frac{M^2}{\mu_R^2}, \frac{\mu_R^2}{\mu^2}, z, \epsilon \right), \end{aligned} \quad (2.20)$$

where we have defined the finite remainder of the soft function as S_{ab}^{fin} . The coefficient \overline{K}_{ab} is resulting from the IR pole part, which only involves the soft divergences in the real contribution. It can be related to Z_{ab}^{IR} as following:

$$\overline{K}_{ab} \left(\hat{a}_s, \frac{\mu_R^2}{\mu^2}, z, \epsilon \right) = -2M^2 \frac{d}{dM^2} \ln Z_{ab}^{\text{IR}} \delta(1-z). \quad (2.21)$$

Expanding them in the bare coupling \hat{a}_s gives:

$$\overline{K}_{ab} \left(\hat{a}_s, \frac{\mu_R^2}{\mu^2}, z, \epsilon \right) = \sum_{k=1} \hat{a}_s^k S_\epsilon^k \left(\frac{\mu_R^2}{\mu^2} \right)^{-k\epsilon} \overline{K}_{ab}^{(k)}(\epsilon) \delta(1-z) = \sum_{k=1} Z_{\alpha_s}^k(\mu_R^2) a_s^k(\mu_R^2) \overline{K}_{ab}^{(k)}(\epsilon) \delta(1-z). \quad (2.22)$$

The coefficient $\overline{K}_{ab}^{(k)}(\epsilon)$ solely depends on the cusp (A_a) anomalous dimension and the beta function. The relationship is given in eq.(35) of ref. [111] by replacing ϵ with -2ϵ and A_k^I

¹¹The 4-loop cusp anomalous dimension has been computed analytically in refs. [103, 104].

¹²The complete 4-loop virtual anomalous dimensions are firstly known in ref. [105] for quarks and in ref. [106] for gluons.

with $A_a^{(k)}$. Further, the renormalisation group invariance of \mathcal{S}_{ab} (i.e., $\frac{d}{d \ln \mu_R^2} \mathcal{S}_{ab}(z, M^2, \mu^2, \epsilon) = 0$) yields:

$$\begin{aligned} \frac{d}{d \ln \mu_R^2} \overline{G}_{ab} &= -\frac{d}{d \ln \mu_R^2} \overline{K}_{ab} = \epsilon \sum_{k=1} k \hat{a}_s^k S_\epsilon^k \left(\frac{\mu_R^2}{\mu^2} \right)^{-k\epsilon} \overline{K}_{ab}^{(k)}(\epsilon) \delta(1-z) \\ &= \epsilon \sum_{k=1} k Z_{\alpha_s}^k(\mu_R^2) a_s^k(\mu_R^2) \overline{K}_{ab}^{(k)}(\epsilon) \delta(1-z) = -A_a \delta(1-z). \end{aligned} \quad (2.23)$$

This is obtained from the peculiar structure of $\ln Z_{ab}^{\text{IR}}(M^2, \mu_R^2, \epsilon)$ with $Z_{ab}^{\text{IR}}(M^2, \mu_R^2, \epsilon) = \sum_{k=1} a_s^k(\mu_R^2) Z_{ab}^{\text{IR},(k)}(M^2, \mu_R^2, \epsilon)$ at every order in the perturbative expansion:

$$\begin{aligned} \frac{d}{d \ln \mu_R^2} \ln Z_{ab}^{\text{IR},(k)}(M^2, \mu_R^2, \epsilon) &= -\frac{1}{2} A_a^{(k)} \ln \left(\frac{-M^2}{\mu_R^2} \right) + B_a^{(k)} + \frac{f_a^{(k)}}{2} \\ &= -\frac{1}{2} A_a^{(k)} \ln \left(\frac{-M^2}{\mu_R^2} \right) - \gamma_a^{\text{collinear},(k)}. \end{aligned} \quad (2.24)$$

$f_a(a_s) = \sum_{k=1} a_s^k f_a^{(k)}$ is called soft/eikonal anomalous dimension ¹³ with $f_a^{(1)} = 0$. Up to three loops in QCD, the cusp and soft anomalous dimension satisfies a Casimir scaling relationship given by $\frac{A_a}{A_q} = \frac{f_a}{f_q} = \frac{C_a}{C_q} = \frac{C_A}{C_F}$. The collinear anomalous dimension, which is analytically known up to 4 loops [113], can be related to the virtual and soft anomalous dimensions via $\gamma_a^{\text{collinear}} = \sum_{k=1} a_s^k \gamma_a^{\text{collinear},(k)} = -B_a - \frac{f_a}{2}$. From eq.(2.23), \overline{G}_{ab} takes the form:

$$\begin{aligned} \overline{G}_{ab} \left(\hat{a}_s, \frac{M^2}{\mu_R^2}, \frac{\mu_R^2}{\mu^2}, z, \epsilon \right) &= \underbrace{\sum_{k=1} \hat{a}_s^k S_\epsilon^k \left(\frac{M^2}{\mu^2} \right)^{-k\epsilon} \overline{G}_{ab}^{(k)}(z, \epsilon)}_{=\overline{G}_{ab} \left(\hat{a}_s, 1, \frac{M^2}{\mu^2}, z, \epsilon \right)} - \underbrace{\delta(1-z) \int_{\frac{M^2}{\mu_R^2}}^1 \frac{d\lambda^2}{\lambda^2} A_a(a_s(\lambda^2 \mu_R^2))}_{=\overline{K}_{ab}(\hat{a}_s, \frac{\mu_R^2}{\mu^2}, z, \epsilon) - \overline{K}_{ab}(\hat{a}_s, \frac{M^2}{\mu^2}, z, \epsilon)}, \end{aligned} \quad (2.25)$$

where the first term on the right-hand side is the boundary term at $\mu_R = M$, whose explicit form is determined from the soft limit of real corrections.

In light of the differential equation (2.20) and the renormalisation group invariance eq.(2.23), the solution takes the form ¹⁴:

$$\ln \mathcal{S}_{ab}(z, M^2, \mu^2, \epsilon) = -\sum_{k=1} \hat{a}_s^k S_\epsilon^k \left(\frac{M^2}{\mu^2} \right)^{-k\epsilon} \frac{1}{k\epsilon} \left(\overline{K}_{ab}^{(k)}(\epsilon) \delta(1-z) + \overline{G}_{ab}^{(k)}(z, \epsilon) \right). \quad (2.26)$$

Alternatively, with an understanding on the structure of $\overline{G}_{ab}^{(k)}(z, \epsilon)$ from the explicit results

$$\overline{G}_{ab}^{(k)}(z, \epsilon) = ((1-z)^2)^{-k\epsilon} \left[\frac{-2k\epsilon}{1-z} \overline{G}_{ab}^{(k)}(\epsilon) + \left(\frac{-2k\epsilon}{1-z} \right)_+ \overline{K}_{ab}^{(k)}(\epsilon) \right], \quad (2.27)$$

¹³The four loop quark soft anomalous dimension is given in ref. [105], while the 4-loop gluon counterpart is obtained in ref. [106] from the quark one with the conjecture that they satisfy the generalised Casimir scaling rule [112].

¹⁴The M^2 independent term in $\ln \mathcal{S}_{ab}(z, M^2, \mu^2, \epsilon)$ from the general solution of the first-order differential equation (2.20) is vanishing.

one can also formulate a better functional form for $\ln \mathcal{S}_{ab}(z, M^2, \mu^2, \epsilon)$:

$$\ln \mathcal{S}_{ab}(z, M^2, \mu^2, \epsilon) = 2 \sum_{k=1} \hat{a}_s^k S_\epsilon^k \left(\frac{M^2(1-z)^2}{\mu^2} \right)^{-k\epsilon} \frac{1}{1-z} \left(\overline{K}_{ab}^{(k)}(\epsilon) + \overline{G}_{ab}^{(k)}(\epsilon) \right), \quad (2.28)$$

which satisfies all the aforementioned differential equations. Here we have used the relationship

$$\begin{aligned} \frac{1}{1-z} [(1-z)^2]^{-k\epsilon} &= \frac{1}{-2k\epsilon} \delta(1-z) + \left[\frac{1}{1-z} ((1-z)^2)^{-k\epsilon} \right]_+ \\ &= \frac{1}{-2k\epsilon} \delta(1-z) + \sum_{j=0} \frac{(-2k\epsilon)^j}{j!} \mathcal{D}_j(z). \end{aligned} \quad (2.29)$$

The exact form of $\overline{G}_{ab}^{(k)}(\epsilon)$ is given in eq.(37) of ref. [111] by replacing ϵ with -2ϵ and identifying the subscript P as S (therefore $\delta_{P,SJ} = 0$). In particular, we have $\overline{G}_{ab}^{(1)}(\epsilon) = \epsilon \frac{3}{2} \zeta_2 A_a^{(1)} + \mathcal{O}(\epsilon^2)$. Equation (2.28) obviously shows that when one takes $\mu \sim \mathcal{O}(M(1-z))$, the soft function is free of any large logarithms, which should take the initial scale of its renormalisation group evolution. The proper initial scale is just at the order around $M(1-z)$, thus suffering from the ambiguities of the initial scale choices. In eq. (2.28), the terms $\left(\frac{M^2(1-z)^2}{\mu^2} \right)^{-\epsilon}$ and $\frac{1}{(1-z)}$ are from two body phase space and the real matrix element squared respectively. For more details on this structure and for explicit results, we refer readers to refs. [107, 111, 114]. The form of the soft function as given in eq. (2.28) is same or universal for any arbitrary production process of colourless final states. This is evident since the soft enhancements only depend on the nature of the external coloured particles, i.e., the initial partons. It is also interesting to find that \mathcal{S}_{ab} satisfies maximally non-abelian property up to third order in the strong coupling constant [107, 111, 115, 116], by which the quark and gluon lines are related by the Casimir constants in the adjoint and fundamental representations. In other words, we have $\frac{\mathcal{S}_{gg}}{\mathcal{S}_{q\bar{q}}} = \frac{C_A}{C_F}$. However, whether the validity of this property holds beyond third order with the so-called generalised Casimir scaling relation [112] needs to be addressed in future. In the present paper, we only need the knowledge of the 3-loop soft function \mathcal{S}_{gg} .

2.3 Threshold resummation

Threshold logarithmic corrections dominate when the partonic scaling variable z approaches to unity. This is manifested in eq. (2.28) in terms of $\{\delta(1-z), \mathcal{D}_i(z)\}$ which is evident by using the relation eq. (2.29). In this kinematic limit, the large logarithm $\ln(1-z)$ multiplying with the small coupling a_s produces $\mathcal{O}(1)$ terms, i.e., $a_s \ln(1-z) \sim \mathcal{O}(1)$. This potentially spoils the perturbative convergence if we truncate at a fixed order in a_s . In such a case, the threshold resummation procedure [117, 118] provides an alternative perturbative expansion.

In order to construct the resummation framework, we employ the structure of soft function \mathcal{S}_{ab} , AP splitting kernel and the master equation (2.15) that we have discussed

in the last subsection. Using the relation eq. (2.29), the soft function can be decomposed into the Dirac delta part and the plus distribution part:

$$\ln \mathcal{S}_{ab} = \ln \mathcal{S}_{ab,\delta} \delta(1-z) + \ln \mathcal{S}_{ab,\mathcal{D}}, \quad (2.30)$$

where $\ln \mathcal{S}_{ab,\delta}$ is proportional to $\delta(1-z)$ and $\ln \mathcal{S}_{ab,\mathcal{D}}$ involves only plus distributions of the form \mathcal{D}_i . Rearranging eq. (2.28), we get:

$$\ln \mathcal{S}_{ab,\delta} = - \sum_{k=1} \hat{a}_s^k S_\epsilon^k \left(\frac{M^2}{\mu^2} \right)^{-k\epsilon} \frac{1}{k\epsilon} \left(\overline{K}_{ab}^{(k)}(\epsilon) + \overline{G}_{ab}^{(k)}(\epsilon) \right). \quad (2.31)$$

The above expression involves ϵ poles and finite terms, where the former will cancel against the IR poles of the virtual correction Z_{ab}^{IR} and of the splitting kernels $\Gamma_{aa}^{-1}, \Gamma_{bb}^{-1}$. Similarly, the distribution part of the soft function is given by:

$$\begin{aligned} \ln \mathcal{S}_{ab,\mathcal{D}} &= 2 \sum_{k=1} \hat{a}_s^k S_\epsilon^k \left(\frac{M^2}{\mu^2} \right)^{-k\epsilon} \left(\frac{(1-z)^{-2k\epsilon}}{1-z} \right)_+ \left(\overline{K}_{ab}^{(k)}(\epsilon) + \overline{G}_{ab}^{(k)}(\epsilon) \right) \\ &= \left(\frac{2}{1-z} \sum_{k=1} a_s^k (M^2(1-z)^2) Z_{\alpha_s}^k (M^2(1-z)^2) \overline{G}_{ab}^{(k)}(\epsilon) \right)_+ \\ &\quad + \left(\frac{2}{1-z} \sum_{k=1} \hat{a}_s^k S_\epsilon^k \left(\frac{\mu_F^2}{\mu^2} \right)^{-k\epsilon} \left[\left(\frac{M^2(1-z)^2}{\mu_F^2} \right)^{-k\epsilon} - 1 \right] \overline{K}_{ab}^{(k)}(\epsilon) \right)_+ \\ &\quad + \left(\frac{2}{1-z} \right)_+ \sum_{k=1} \hat{a}_s^k S_\epsilon^k \left(\frac{\mu_F^2}{\mu^2} \right)^{-k\epsilon} \overline{K}_{ab}^{(k)}(\epsilon). \end{aligned} \quad (2.32)$$

This gives us an integral representation for $\ln \mathcal{S}_{ab,\mathcal{D}}$:

$$\begin{aligned} \ln \mathcal{S}_{ab,\mathcal{D}} &= 2 \left(\frac{1}{1-z} \left\{ \int_{\mu_F^2}^{M^2(1-z)^2} \frac{d\lambda^2}{\lambda^2} A_a(a_s(\lambda^2)) + \overline{\mathcal{G}}_{ab}(a_s(M^2(1-z)^2), \epsilon) \right\} \right)_+ \\ &\quad + \left(\frac{2}{1-z} \right)_+ \sum_{k=1} \hat{a}_s^k S_\epsilon^k \left(\frac{\mu_F^2}{\mu^2} \right)^{-k\epsilon} \overline{K}_{ab}^{(k)}(\epsilon), \end{aligned} \quad (2.33)$$

where $\overline{\mathcal{G}}_{ab}(a_s(\mu_R^2), \epsilon)$ is

$$\overline{\mathcal{G}}_{ab}(a_s(\mu_R^2), \epsilon) \equiv \sum_{k=1} a_s^k(\mu_R^2) Z_{\alpha_s}^k(\mu_R^2) \overline{G}_{ab}^{(k)}(\epsilon). \quad (2.34)$$

In eq. (2.33), we have used the relation

$$\sum_{k=1} \hat{a}_s^k S_\epsilon^k \left(\frac{\mu_F^2}{\mu^2} \right)^{-k\epsilon} \left[\left(\frac{M^2}{\mu_F^2} \right)^{-k\epsilon} - 1 \right] \overline{K}_{ab}^{(k)}(\epsilon) = \int_{\mu_F^2}^{M^2} \frac{d\lambda^2}{\lambda^2} A_a(a_s(\lambda^2)). \quad (2.35)$$

The IR poles in the second line in eq. (2.33) cancel against the poles of the \mathcal{D}_0 term of the splitting kernels exactly. The finite remnants of the splitting kernels depend on $\ln(\mu_F^2/\mu_R^2)$ when expressing eq. (2.19) in the renormalised coupling constant a_s at the scale μ_R .

Convoluting the soft function with the AP splitting kernels and Z_{ab}^{IR} produces the IR finite function $S_{\Gamma,ab}$ defined in eq. (2.16):

$$\ln S_{\Gamma,ab}(z, M^2, \mu_F^2, \mu_R^2) = 2 \ln Z_{ab}^{\text{IR}} \delta(1-z) + 2 \ln \mathcal{S}_{ab,\delta} \delta(1-z) + 2 \ln \mathcal{S}_{ab,\mathcal{D}} - \ln \Gamma_{aa} - \ln \Gamma_{bb}. \quad (2.36)$$

As mentioned above, the poles of $\ln \mathcal{S}_{ab,\delta}$ and $\ln \mathcal{S}_{ab,\mathcal{D}}$ cancel against the respective terms from Z_{ab}^{IR} , Γ_{aa} and Γ_{bb} . Decomposing the splitting kernels into the Dirac delta and plus distribution parts:

$$\ln \Gamma_{aa} = \ln \Gamma_{aa,\delta} \delta(1-z) + \ln \Gamma_{aa,\mathcal{D}}, \quad (2.37)$$

and further expressing the soft function and the splitting kernels into the singular and finite terms:

$$\begin{aligned} \ln \mathcal{S}_{ab,\{\delta,\mathcal{D}\}} &= \ln \mathcal{S}_{ab,\{\delta,\mathcal{D}\}}^{\text{sing}} + \ln \mathcal{S}_{ab,\{\delta,\mathcal{D}\}}^{\text{fin}}, \\ \ln \Gamma_{aa,\{\delta,\mathcal{D}\}} &= \ln \Gamma_{aa,\{\delta,\mathcal{D}\}}^{\text{sing}} + \ln \Gamma_{cc,\{\delta,\mathcal{D}\}}^{\text{fin}}, \end{aligned} \quad (2.38)$$

$S_{\Gamma,ab}$ becomes ¹⁵:

$$\begin{aligned} \ln S_{\Gamma,ab}(z, M^2, \mu_F^2, \mu_R^2) &= \left(2 \ln \mathcal{S}_{ab,\delta}^{\text{fin}} - \ln \Gamma_{aa,\delta}^{\text{fin}} - \ln \Gamma_{bb,\delta}^{\text{fin}} \right) \delta(1-z) + \left(2 \ln \mathcal{S}_{ab,\mathcal{D}}^{\text{fin}} - \ln \Gamma_{aa,\mathcal{D}}^{\text{fin}} - \ln \Gamma_{bb,\mathcal{D}}^{\text{fin}} \right) \\ &= \left(2 \ln \mathcal{S}_{ab,\delta}^{\text{fin}} - \ln \Gamma_{aa,\delta}^{\text{fin}} - \ln \Gamma_{bb,\delta}^{\text{fin}} \right) \delta(1-z) \\ &\quad + \left(\frac{2}{1-z} \left\{ \int_{\mu_F^2}^{M^2(1-z)^2} \frac{d\lambda^2}{\lambda^2} A_a(a_s(\lambda^2)) + \bar{\mathcal{G}}_{ab}(a_s(M^2(1-z)^2)) \right\} \right)_+, \end{aligned} \quad (2.39)$$

where we have defined

$$\bar{\mathcal{G}}_{ab}(a_s(M^2(1-z)^2)) \equiv \lim_{\epsilon \rightarrow 0} \bar{\mathcal{G}}_{ab}(a_s(M^2(1-z)^2), \epsilon). \quad (2.40)$$

Here, the first line comprises of the finite part of $\ln \mathcal{S}_{ab,\delta}$ and the finite remnants arising from the $\delta(1-z)$ terms of the splitting kernels.

Finally, taking into account the finite hard function H_{ab} , as in eq. (2.15), it gives us the partonic coefficient function:

$$\begin{aligned} \Delta_{ab}^{\text{SV}}(z, M^2, \mu_F^2) &= g_{0,ab}(M^2, \mu_F^2, \mu_R^2) \delta(1-z) \otimes \\ &\quad \mathcal{P} \exp \left(\frac{2}{1-z} \left\{ \int_{\mu_F^2}^{M^2(1-z)^2} \frac{d\lambda^2}{\lambda^2} A_a(a_s(\lambda^2)) + \bar{\mathcal{G}}_{ab}(a_s(M^2(1-z)^2)) \right\} \right)_+, \end{aligned} \quad (2.41)$$

where

$$g_{0,ab}(M^2, \mu_F^2, \mu_R^2) \equiv H_{ab}(M^2, \mu_R^2) \times \exp \left(2 \ln \mathcal{S}_{ab,\delta}^{\text{fin}} - \ln \Gamma_{aa,\delta}^{\text{fin}} - \ln \Gamma_{bb,\delta}^{\text{fin}} \right). \quad (2.42)$$

¹⁵Note that since $S_{\Gamma,ab}$ is IR finite, we can take $\epsilon = 0$ directly for all the quantities appearing in it.

The symbol \mathcal{P} refers to the operator for the “path-ordered exponential”, which has the following expansion for an arbitrary function $f(z)$:

$$\mathcal{P}e^{f(z)} = \delta(1-z) + \frac{1}{1!}f(z) + \frac{1}{2!}(f(z) \otimes f(z)) + \dots \quad (2.43)$$

The second line in eq. (2.41) involves enhanced logarithms in the limit $z \rightarrow 1$ which have been resummed. Since this term is in the form of convolutions, it is convenient to solve it in the Mellin N -space, where all the convolutions turn into normal products. The Mellin transform of a function $f(z)$ is generally defined as:

$$\mathcal{M}[f(z)](N) \equiv \int_0^1 dz z^{N-1} f(z). \quad (2.44)$$

The threshold limit $z \rightarrow 1$ corresponds to $N \rightarrow \infty$ in the Mellin N -space. Note that $\mathcal{M}[\delta(1-z)] = 1$ and $\mathcal{M}[\mathcal{D}_k(z)] = \frac{(-1)^{k+1}}{(k+1)} \ln^{k+1} N + \mathcal{O}(\ln^k N)$. In the Mellin space, eq. (2.41) reads as:

$$\begin{aligned} \Delta_{ab}^{\text{res}}(N, M^2, \mu_F^2) &\equiv \int_0^1 dz z^{N-1} \Delta_{ab}^{\text{SV}}(z, M^2, \mu_F^2) \\ &= g_{0,ab}(M^2, \mu_F^2, \mu_R^2) \times \\ &\quad \exp \left[2 \int_0^1 dz \frac{z^{N-1} - 1}{1-z} \left(\int_{\mu_F^2}^{M^2(1-z)^2} \frac{d\lambda^2}{\lambda^2} A_a(a_s(\lambda^2)) + \bar{\mathcal{G}}_{ab}(a_s(M^2(1-z)^2)) \right) \right]. \end{aligned} \quad (2.45)$$

Solving the above integral in the Mellin space with an expansion over the resummation parameter $\omega \equiv 2\beta_0 a_s(\mu_R^2) \ln N$ results into:

$$\begin{aligned} \Delta_{ab}^{\text{res}}(N, M^2, \mu_F^2) &= g_{0,ab}(M^2, \mu_F^2, \mu_R^2) \times \\ &\quad \exp \left(\tilde{C}_{0,ab}(a_s(\mu_R^2)) + g_{1,ab}(\omega) \ln N + \sum_{k=2} a_s^{k-2}(\mu_R^2) g_{k,ab}(\omega) \right). \end{aligned} \quad (2.46)$$

As been noticed from the above equation, the exponent after the Mellin transform has an additional N -independent coefficient, $\tilde{C}_{0,ab}$, arising from the $\mathcal{O}(1)$ terms of $\mathcal{M}[\mathcal{D}_k(z)]$. This coefficient is in general depending on the Riemann zeta function ζ_n and the Euler-Mascheroni constant γ_E . Furthermore, the N -dependent functions $g_{k,ab}$, $k \geq 1$ are all-order coefficients expressed in terms of $\omega \sim \mathcal{O}(1)$. These coefficients satisfy the condition that they vanish in the limit $N \rightarrow 1$. Their dependencies on $\ln \frac{M^2}{\mu_R^2}$ and $\ln \frac{M^2}{\mu_F^2}$ are also implicitly understood. Taking out all the N -independent terms from the exponent gives us:

$$\Delta_{ab}^{\text{res}}(N, M^2, \mu_F^2) = \tilde{g}_{0,ab}(M^2, \mu_F^2, \mu_R^2) \exp \left(g_{1,ab}(\omega) \ln N + \sum_{k=2} a_s^{k-2}(\mu_R^2) g_{k,ab}(\omega) \right). \quad (2.47)$$

The total N -independent prefactor is

$$\begin{aligned} \tilde{g}_{0,ab}(M^2, \mu_F^2, \mu_R^2) &\equiv g_{0,ab}(M^2, \mu_F^2, \mu_R^2) \exp \left(\tilde{C}_{0,ab}(a_s(\mu_R^2)) \right) \\ &= H_{ab}(M^2, \mu_R^2) \times \exp \left(2 \ln \mathcal{S}_{ab,\delta}^{\text{fin}} - \ln \Gamma_{aa,\delta}^{\text{fin}} - \ln \Gamma_{bb,\delta}^{\text{fin}} + \tilde{C}_{0,ab} \right). \end{aligned} \quad (2.48)$$

As stated earlier, the resummation coefficients $g_{k,ab}(\omega)$ are universal and depend only on the nature of incoming partons. However, $\tilde{g}_{0,ab}$ is process dependent. It can be expanded in $a_s(\mu_R^2)$ as

$$\tilde{g}_{0,ab}(M^2, \mu_F^2, \mu_R^2) = a_s^b(\mu_R^2) \sum_{k=0} a_s^k(\mu_R^2) \tilde{g}_{0,ab}^{(k)}(M^2, \mu_F^2, \mu_R^2). \quad (2.49)$$

Each term in the exponent in eq. (2.47) has been resummed to all orders in α_s . At the N^k LL accuracy, we should take into account both the logarithmic terms up to $g_{k+1,ab}(\omega)$ in the exponent and the N -independent terms up to $\tilde{g}_{0,ab}^{(k)}$ in $\tilde{g}_{0,ab}$. It is also implicitly understood that the hard function, as well as $g_{0,ab}$ and $\tilde{g}_{0,ab}$, may depend on the other underlying Born kinematic variables, which we have not yet explicitly written out.

When the resummation calculations match to the fixed-order computations, we need to subtract the double counting between the two. At the N^k LO + N^k LL accuracy, the double counting is just the N^k LO soft-virtual term encoded in the partonic coefficient function. In other words, it is the $a_s(\mu_R^2)$ series of Δ_{ab}^{res} ¹⁶ up to the $\mathcal{O}(a_s^{b+k})$ term.

2.4 Ambiguities in resummation and resummation schemes

Up to a given logarithmic accuracy, the right-hand side of the resummation formalism eq. (2.47) is not uniquely defined. One has the freedom to choose which N -independent piece should be absorbed into the exponent. In other words, we can rewrite the resummed N^k LO partonic coefficient function in the Mellin space as

$$\begin{aligned} \Delta_{ab}^{\text{res}}(N, M^2, \mu_F^2) \Big|_{N^k\text{LL}} &= \left[\tilde{g}_{0,ab}(M^2, \mu_F^2, \mu_R^2) \exp\left(-\ddot{C}_{0,ab}(M^2, \mu_F^2, \mu_R^2)\right) \right]_{N^k\text{LO}} \quad (2.50) \\ &\times \exp\left(\ddot{C}_{0,ab}(M^2, \mu_F^2, \mu_R^2) + g_{1,ab}(\omega) \ln N + \sum_{j=2}^{k+1} a_s^{j-2}(\mu_R^2) g_{j,ab}(\omega)\right), \end{aligned}$$

where the function $\ddot{C}_{0,ab}(M^2, \mu_F^2, \mu_R^2)$ is an arbitrary N -independent function that can be expressed in an $a_s(\mu_R^2)$ series. The subscript N^k LO means that the whole expression in the bracket should be kept up to the first $k+1$ terms in the a_s series. This essentially leads to the ambiguities in the threshold resummation formalism at a given logarithmic accuracy.¹⁷ In this subsection, we present a few concrete forms of $\ddot{C}_{0,ab}$ to discuss such ambiguities. First of all, in eq. (2.47), we resum the large logarithms of the form $\ln N$, with the resummation parameter given by ω . However, it is observed that in the large N -expansion, $\ln N$ is always associated with the Euler-Mascheroni constant γ_E . Alternatively, one usually takes the resummation parameter as $\bar{\omega} \equiv 2\beta_0 a_s(\mu_R^2) \ln \bar{N}$ with $\bar{N} \equiv N e^{\gamma_E}$. In this paper, we consider four different resummation schemes as follows.

¹⁶Note that ω also depends on $a_s(\mu_R^2)$, and it should be expanded into the a_s series too.

¹⁷Such resummation ambiguities have already been studied in the Drell-Yan process at N^3 LL accuracy in ref. [119].

- N_1 scheme : In this scheme, we have the $N^k\text{LL}$ resummed partonic coefficient directly from eq. (2.47)

$$\begin{aligned} \Delta_{ab}^{\text{res},N_1}(N, M^2, \mu_F^2) \Big|_{N^k\text{LL}} &= [\tilde{g}_{0,ab}(M^2, \mu_F^2, \mu_R^2)]_{N^k\text{LO}} \\ &\times \exp \left(g_{1,ab}(\omega) \ln N + \sum_{j=2}^{k+1} a_s^{j-2}(\mu_R^2) g_{j,ab}(\omega) \right). \end{aligned} \quad (2.51)$$

- N_2 scheme : In this scheme, we take $\ddot{C}_{0,ab}(M^2, \mu_F^2, \mu_R^2) = \tilde{C}_{0,ab,\zeta} \equiv \lim_{\gamma_E \rightarrow 0} \tilde{C}_{0,ab}$. In other words, $\tilde{C}_{0,ab,\zeta}$ solely depends on the Riemann zeta function, and is defined as $\tilde{C}_{0,ab}$ by removing the γ_E -dependent terms. Similarly, we can define $\tilde{C}_{0,ab,\gamma_E} \equiv \tilde{C}_{0,ab} - \tilde{C}_{0,ab,\zeta} \propto \gamma_E$. Then, the $N^k\text{LL}$ resummed partonic coefficient becomes

$$\begin{aligned} \Delta_{ab}^{\text{res},N_2}(N, M^2, \mu_F^2) \Big|_{N^k\text{LL}} &= \left[H_{ab}(M^2, \mu_F^2) \exp \left(2 \ln \mathcal{S}_{ab,\delta}^{\text{fin}} - \ln \Gamma_{aa,\delta}^{\text{fin}} - \ln \Gamma_{bb,\delta}^{\text{fin}} + \tilde{C}_{0,ab,\gamma_E} \right) \right]_{N^k\text{LO}} \\ &\times \exp \left[\left(\tilde{C}_{0,ab,\zeta} \right)_{N^{k-1}\text{LO}} \right] \exp \left(g_{1,ab}(\omega) \ln N + \sum_{j=2}^{k+1} a_s^{j-2}(\mu_R^2) g_{j,ab}(\omega) \right). \end{aligned} \quad (2.52)$$

In eq. (2.52), we use the subscript $N^{k-1}\text{LO}$ in the exponent because the lowest order of $\tilde{C}_{0,ab,\zeta}$ is $\mathcal{O}(a_s)$.

- \bar{N}_1 scheme : In this scheme, we use the resummation parameter $\bar{\omega}$ instead of ω . The coefficient is

$$\begin{aligned} \Delta_{ab}^{\text{res},\bar{N}_1}(N, M^2, \mu_F^2) \Big|_{N^k\text{LL}} &= [\bar{g}_{0,ab}(M^2, \mu_F^2, \mu_R^2)]_{N^k\text{LO}} \\ &\times \exp \left(\bar{g}_{1,ab}(\bar{\omega}) \ln \bar{N} + \sum_{j=2}^{k+1} a_s^{j-2}(\mu_R^2) \bar{g}_{j,ab}(\bar{\omega}) \right), \end{aligned} \quad (2.53)$$

where $\bar{g}_{j,ab}(\bar{\omega}) = [\lim_{\gamma_E \rightarrow 0} g_{j,ab}(\omega)]_{\omega \rightarrow \bar{\omega}}$ when $j \geq 1$. This means that we have taken

$$\begin{aligned} \ddot{C}_{0,ab}(M^2, \mu_F^2, \mu_R^2) &= \left(\bar{g}_{1,ab}(\bar{\omega}) \ln \bar{N} + \sum_{j=2}^{k+1} a_s^{j-2}(\mu_R^2) \bar{g}_{j,ab}(\bar{\omega}) \right) \\ &- \left(g_{1,ab}(\omega) \ln N + \sum_{j=2}^{k+1} a_s^{j-2}(\mu_R^2) g_{j,ab}(\omega) \right). \end{aligned} \quad (2.54)$$

It can be proven that $\ddot{C}_{0,ab}(M^2, \mu_F^2, \mu_R^2)$ is indeed independent of N . Thus, $\bar{g}_{0,ab}(M^2, \mu_F^2, \mu_R^2) = \tilde{g}_{0,ab}(M^2, \mu_F^2, \mu_R^2) \exp \left(-\ddot{C}_{0,ab}(M^2, \mu_F^2, \mu_R^2) \right)$.

- \overline{N}_2 scheme : In this scheme, we have the coefficient

$$\begin{aligned} \Delta_{ab}^{\text{res}, \overline{N}_2}(N, M^2, \mu_F^2) \Big|_{N^k \text{LL}} &= \left[H_{ab}(M^2, \mu_R^2) \exp \left(2 \ln \mathcal{S}_{ab, \delta}^{\text{fin}} - \ln \Gamma_{aa, \delta}^{\text{fin}} - \ln \Gamma_{bb, \delta}^{\text{fin}} \right) \right]_{N^k \text{LO}} \\ &\times \exp \left[\left(\tilde{C}_{0, ab, \zeta} \right)_{N^{k-1} \text{LO}} \right] \exp \left(\bar{g}_{1, ab}(\bar{\omega}) \ln \bar{N} + \sum_{j=2}^{k+1} a_s^{j-2}(\mu_R^2) \bar{g}_{j, ab}(\bar{\omega}) \right). \end{aligned} \quad (2.55)$$

Notice that in this scheme the γ_E -dependent piece $\tilde{C}_{0, ab, \gamma_E}$ has been absorbed into the transforms of $N \rightarrow \bar{N}$ and $\omega \rightarrow \bar{\omega}$ in the exponent.

2.5 $N^3\text{LL}$ resummation for Higgs boson pair production

With the general formalism for the threshold resummation of any colourless final state, we are now in the position to say something specifically for the Higgs pair production in ggF. We begin with the master formula for the threshold resummation given in eq. (2.47). The quantities in the exponent given by $g_{k, gg}(\omega)$ are known up to $k \leq 4$,¹⁸ which were first applied for the single Higgs production up to the $N^3\text{LL}$ accuracy [121]. These expressions can be fully recycled for the Higgs boson pair process. Their expressions up to the fourth order are provided in appendix A for the completeness.

The N -independent coefficient $\tilde{g}_{0, gg}$ is not universal, whose process dependence is only stemming from the hard function H_{gg} . The universal N -independent contributions from the soft function and the splitting kernels could be found in appendices D and E of ref. [114]. For the convenience of reader, we also provide their explicit results for the ggF processes up to the three loops in appendix A. Combining them together with the hard function returns $\tilde{g}_{0, gg}^{(k)}$ appearing in eq. (2.49).

The hard function H_{gg} up to 3 loops for the $N^3\text{LL}$ threshold resummation of the di-Higgs process in the infinite top quark mass approximation has been documented in appendix A of ref. [52]. For the sake of completeness, we still briefly mentioned it here. The effective Lagrangian given in eq.(2.1) of ref. [52] contains two Wilson coefficients C_h

¹⁸The explicit result of $\bar{g}_{4, gg}(\bar{\omega})$ in eq. (2.53) can also be found in appendix G of ref. [114] by replacing ω with $\bar{\omega}$. Their general expressions for both quarks and gluons are in principle also given, e.g., in ref. [120].

and C_{hh} . These coefficients up to $\mathcal{O}(a_s^4)$ are:

$$\begin{aligned}
C_h = & -\frac{4a_s}{3} \left\{ 1 + 11a_s + a_s^2 \left[\frac{2777}{18} - \frac{67}{6}n_q + L_t \left(19 + \frac{16}{3}n_q \right) \right] \right. \\
& + a_s^3 \left[-\frac{2761331}{648} + \zeta_3 \frac{897943}{144} + \left(\frac{58723}{324} - \zeta_3 \frac{110779}{216} \right) n_q - \frac{6865}{486} n_q^2 \right. \\
& \left. \left. + L_t \left(\frac{4834}{9} + \frac{2912}{27}n_q + \frac{77}{27}n_q^2 \right) + L_t^2 \left(209 + 46n_q - \frac{32}{9}n_q^2 \right) \right] \right\}, \quad (2.56)
\end{aligned}$$

$$\begin{aligned}
C_{hh} = & -\frac{4a_s}{3} \left\{ 1 + 11a_s + a_s^2 \left[\frac{3197}{18} - \frac{1}{2}n_q + L_t \left(19 + \frac{16}{3}n_q \right) \right] \right. \\
& + a_s^3 \left[-\frac{2633363}{648} + \zeta_3 \frac{897943}{144} + \left(\frac{110611}{324} - \zeta_3 \frac{110779}{216} \right) n_q - \frac{4093}{486} n_q^2 \right. \\
& \left. \left. + L_t \left(\frac{11902}{9} + \frac{7496}{27}n_q - \frac{307}{27}n_q^2 \right) + L_t^2 \left(209 + 46n_q - \frac{32}{9}n_q^2 \right) \right] \right\} \quad (2.57)
\end{aligned}$$

with $L_t \equiv \ln(\mu_R^2/m_t^2)$ and m_t is the on-shell top quark mass. It is important to notice that the Wilson coefficients are at least $\mathcal{O}(a_s)$. Thus, we can organise the amplitude square into three parts dubbed as class- a , b , c , which feature 2, 3, and 4 insertions of the effective vertices respectively. This means that the hard function can be written as

$$H_{gg} = H_{gg}^a + H_{gg}^b + H_{gg}^c, \quad (2.58)$$

whose expressions in terms of the amplitudes are given in eq. (A.10) of ref. [52]. The class- a hard function H_{gg}^a has the similar topologies as the single Higgs process, known up to four loops [122]. The class- b and - c hard functions need the knowledge of other topologies. In eq. (A.6) of ref. [52], besides the trivial typo $\mathcal{M}_i^{B,(1)}$ that should be $\mathcal{M}_i^{B,(1),fin}$, $\mathcal{M}_i^{B,(2),fin}$ should be the finite 2-loop amplitude defined in eq. (2.24) of ref. [64] times $\frac{9C_h^2}{16a_s^2}$. The analytic expression of $\mathcal{M}_i^{B,(2),fin}$ is too lengthy to be directly used in the numerical code. In our calculation, for the practical usage, we have to generate the numerical grids in MATHEMATICA with 100-digit precision and with the help of the package POLYLOGTOOLS [123] first. By knowing the hard function, the N -independent coefficient $\tilde{g}_{0,gg}$ in eq. (2.48) becomes:

$$\begin{aligned}
\tilde{g}_{0,gg}(m_{hh}^2, \mu_F^2, \mu_R^2) &= (H_{gg}^a + H_{gg}^b + H_{gg}^c) \exp \left(2 \ln \mathcal{S}_{gg,\delta}^{fin} - 2 \ln \Gamma_{gg,\delta}^{fin} + \tilde{C}_{0,gg} \right) \\
&= a_s^2(\mu_R^2) \sum_{k=0} a_s^k(\mu_R^2) \tilde{g}_{0,gg}^{(k)}(m_{hh}^2, \mu_F^2, \mu_R^2), \quad (2.59)
\end{aligned}$$

where m_{hh} is the invariant mass of the Higgs pair. The lowest orders of $H_{gg}^a, H_{gg}^b, H_{gg}^c$ contribute to $\tilde{g}_{0,gg}^{(0)}, \tilde{g}_{0,gg}^{(1)}$, and $\tilde{g}_{0,gg}^{(2)}$ respectively.

We have carefully checked our implementation. For example, the hard function has been checked against ref. [52], and its scale dependence satisfies the renormalisation group equation. In order to verify our numerical setup, we have also tested the N³LL resummation calculation of the single Higgs process with ref. [124]. In the N₁ scheme, we find good agreements with ref. [73] at the NNLL accuracy for the di-Higgs process.

3 Results

Before we present our results, we fix our setup for the numerical calculation. In order to recycle the N³LO results that we have calculated before, we take the same setup as in ref. [52]. Namely, we take the Higgs mass $m_h = 125$ GeV and the vacuum expectation value of the Higgs field $v = (\sqrt{2}G_F)^{-\frac{1}{2}} = 246.2$ GeV. The top-quark pole mass $m_t = 173$ GeV enters only into the Wilson coefficients C_h and C_{hh} of the effective Lagrangian. The same PDF PDF4LHC15_nnlo_30 [125–128], along with its α_s renormalisation group running, provided by LHAPDF6 [129] will be used regardless of the α_s or logarithmic order we are considering. The default central scale is chosen as the half of the invariant mass of the Higgs boson pair, i.e., $\mu_0 = m_{hh}/2$. The scale uncertainty, for estimating the missing higher order terms, is evaluated through taking the envelope of the 7-point variations of the factorisation scale μ_F and the renormalisation scale μ_R in the form of $\mu_{R/F} = \xi_{R/F}\mu_0$ with $\xi_{R/F} \in \{0.5, 1, 2\}$ after excluding the two extreme points $(\xi_R, \xi_F) = (0.5, 2), (2, 0.5)$.

3.1 Impact of QCD corrections in the infinite top quark mass approximation

We study the cross sections in the infinite top quark mass limit in this subsection. Both the inclusive cross sections and the Higgs pair invariant mass distributions will be reported.

Let us first focus on the inclusive cross sections that have been integrated with the whole phase space. As aforementioned, in the resummation calculations, we have the additional theoretical uncertainties stemming from the ambiguities in the resummation formalism discussed in subsection 2.4. Figure 2 reports the resummed results from NLO+NLL to N³LO+N³LL in the four typical center-of-mass energies covering the energy ranges of the LHC ($\sqrt{s} = 13, 14$ TeV) and future colliders ($\sqrt{s} = 27, 100$ TeV). Concrete numbers can also be read from table 1. The four resummation schemes, dubbed as $N_1, N_2, \bar{N}_1, \bar{N}_2$, have been defined in subsection 2.4. We have checked our NLL and NNLL calculations against those in ref. [73], where the latter only provides the N_1 results. As anticipated, such a scheme dependence reduces from NLO+NLL to N³LO+N³LL. However, the different schemes give us both the different central values and error bars due to 7-point scale variations. In particular, the differences are more significant between \bar{N}_1 and \bar{N}_2 schemes than \bar{N}_1 vs N_1 or \bar{N}_2 vs N_2 . The scale uncertainties are reduced only marginally from N^kLO to N^kLO+N^kLL in the N_1 and \bar{N}_1 schemes, while a factor two reductions have been observed in the N_2 and \bar{N}_2 schemes. For example, the N³LO error bars are almost same after including the N³LL resummation in the \bar{N}_1 scheme. Besides the scale uncertainties, it is interesting to notice that the central values of N^kLO+N^kLL in the N_2 and \bar{N}_2 schemes are much closer to N^{k+1}LO than the other two. This potentially tells us that our best results N³LO+N³LL in the former two schemes can be extrapolated to predict the next order calculation, i.e., the unknown next-to-next-to-next-to-next-to-leading order (N⁴LO). Although it seems that the N_2 and \bar{N}_2 schemes are equivalently good from the above perspectives, we decide to choose the \bar{N}_2 scheme in the following context as our best predictions, whose scale errors are more symmetric than the N_2 scheme. We want to stress that it is just our choice without any preference from first principles. An alternative attitude that is more conservative is to quote the theoretical uncertainties due to the scheme dependence instead

of picking up one scheme. For instance, if we take the envelope of the $N^3\text{LO}+N^3\text{LL}$ central values in the four schemes, we have $\sigma_{N^3\text{LO}+N^3\text{LL}} = 38.70 \left(\begin{smallmatrix} +0.85\% \\ -0.87\% \end{smallmatrix} \right)_{\text{scale}} \left(\begin{smallmatrix} +0.08\% \\ -0.39\% \end{smallmatrix} \right)_{\text{scheme}}$ fb at 14 TeV, where the second error due to the resummation scheme ambiguities is in anyway subdominant. Alternatively, if one takes the envelope of all the predictions in different schemes including the corresponding scale uncertainties, the cross section at 14 TeV becomes $\sigma_{N^3\text{LO}+N^3\text{LL}} = 38.70 \left(\begin{smallmatrix} +0.89\% \\ -2.6\% \end{smallmatrix} \right)_{\text{scale+scheme}}$ fb. Nevertheless, according to the aforementioned arguments, we will stick to the \bar{N}_2 scheme for the following discussions.

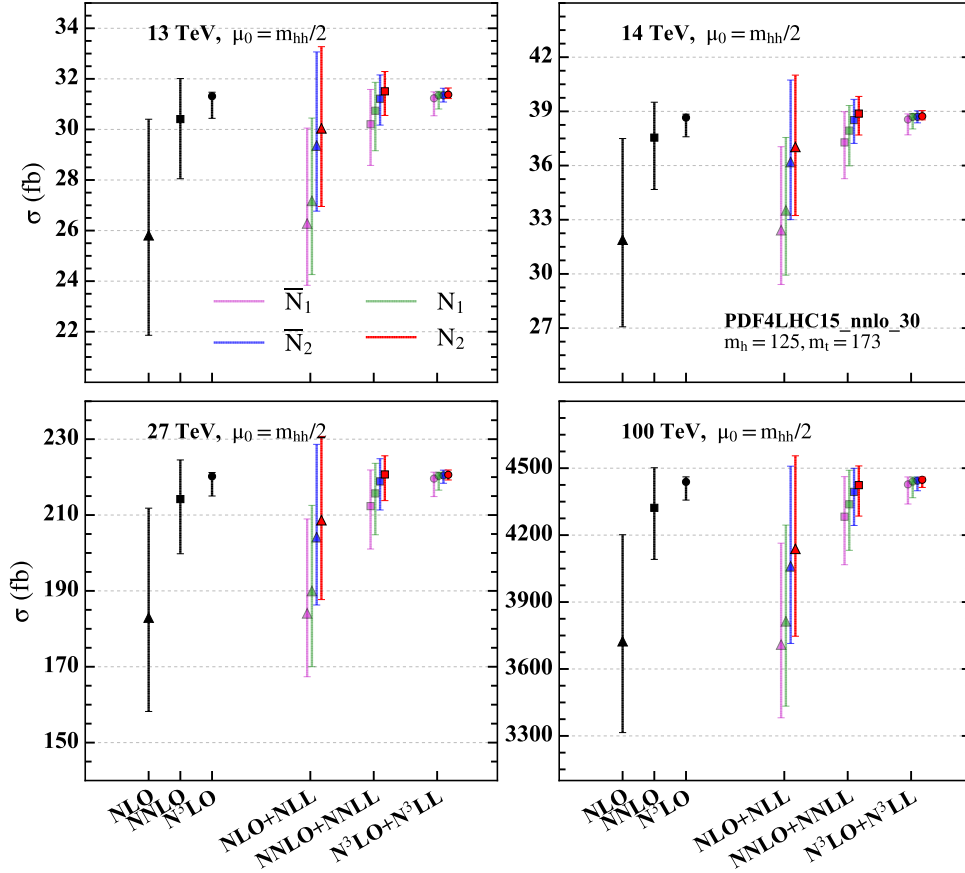


Figure 2: The comparisons of the inclusive cross sections between the fixed order $N^k\text{LO}$ calculations (black) and the threshold resummed $N^k\text{LO}+N^k\text{LL}$ calculations (coloured) at four different energies $\sqrt{s} = 13, 14, 27, 100$ TeV. In each resummation calculation, we have shown four different results stemming from the resummation schemes. They are N_1 (green), N_2 (red), \bar{N}_1 (purple), and \bar{N}_2 (blue) schemes. The error bars are from 7-point scale variations.

Table 1 tells us $N^3\text{LO}+N^3\text{LL}$ cross sections are enhanced only by the permille amounts from $N^3\text{LO}$. This corroborates and further consolidates our previous conclusion that the asymptotic convergence in α_s has reached at $N^3\text{LO}$ [51, 52]. The scale uncertainties

\sqrt{s} [TeV]	Order k	$N^k\text{LO}$	$N^k\text{LO}+N^k\text{LL}$			
			N_1 scheme	N_2 scheme	\bar{N}_1 scheme	\bar{N}_2 scheme
13	0	$13.80^{+31\%}_{-22\%}$	$16.01^{+32\%}_{-23\%}$	$16.01^{+32\%}_{-23\%}$	$21.02^{+36\%}_{-24\%}$	$21.02^{+36\%}_{-24\%}$
	1	$25.81^{+18\%}_{-15\%}$	$27.17^{+12.1\%}_{-10.7\%}$	$30.04^{+10.8\%}_{-10.3\%}$	$26.30^{+14.4\%}_{-9.3\%}$	$29.36^{+12.6\%}_{-8.8\%}$
	2	$30.41^{+5.3\%}_{-7.8\%}$	$30.74^{+3.7\%}_{-5.1\%}$	$31.51^{+2.5\%}_{-3.0\%}$	$30.20^{+4.6\%}_{-5.4\%}$	$31.21^{+3.0\%}_{-3.3\%}$
	3	$31.31^{+0.50\%}_{-2.8\%}$	$31.34^{+0.51\%}_{-1.7\%}$	$31.37^{+0.84\%}_{-0.49\%}$	$31.23^{+0.81\%}_{-2.2\%}$	$31.35^{+0.88\%}_{-0.85\%}$
14	0	$17.06^{+31\%}_{-22\%}$	$19.72^{+32\%}_{-23\%}$	$19.72^{+32\%}_{-23\%}$	$25.80^{+35\%}_{-24\%}$	$25.80^{+35\%}_{-24\%}$
	1	$31.89^{+18\%}_{-15\%}$	$33.52^{+12\%}_{-10.7\%}$	$37.03^{+10.7\%}_{-10.3\%}$	$32.42^{+14.3\%}_{-9.3\%}$	$36.19^{+12.5\%}_{-8.8\%}$
	2	$37.55^{+5.2\%}_{-7.6\%}$	$37.93^{+3.7\%}_{-5.1\%}$	$38.88^{+2.4\%}_{-3.0\%}$	$37.28^{+4.5\%}_{-5.4\%}$	$38.52^{+3.0\%}_{-3.4\%}$
	3	$38.65^{+0.50\%}_{-2.7\%}$	$38.69^{+0.50\%}_{-1.7\%}$	$38.73^{+0.81\%}_{-0.51\%}$	$38.55^{+0.80\%}_{-2.2\%}$	$38.70^{+0.85\%}_{-0.87\%}$
27	0	$98.22^{+26\%}_{-19\%}$	$110.6^{+27\%}_{-20\%}$	$110.6^{+27\%}_{-20\%}$	$141.1^{+29\%}_{-21\%}$	$141.1^{+29\%}_{-21\%}$
	1	$183.0^{+16\%}_{-14\%}$	$190.0^{+11.9\%}_{-10.5\%}$	$208.6^{+10.6\%}_{-10\%}$	$184.1^{+13.5\%}_{-9.1\%}$	$204.2^{+12.0\%}_{-8.8\%}$
	2	$214.2^{+4.8\%}_{-6.7\%}$	$215.7^{+3.7\%}_{-5.1\%}$	$220.7^{+2.2\%}_{-3.1\%}$	$212.3^{+4.5\%}_{-5.3\%}$	$218.9^{+2.7\%}_{-3.4\%}$
	3	$220.2^{+0.46\%}_{-2.3\%}$	$220.3^{+0.44\%}_{-1.7\%}$	$220.6^{+0.57\%}_{-0.62\%}$	$219.6^{+0.77\%}_{-2.2\%}$	$220.4^{+0.63\%}_{-0.94\%}$
100	0	$2015^{+19\%}_{-15\%}$	$2195^{+19\%}_{-15\%}$	$2195^{+19\%}_{-15\%}$	$2697^{+21\%}_{-17\%}$	$2697^{+21\%}_{-17\%}$
	1	$3724^{+13\%}_{-11\%}$	$3813^{+11.3\%}_{-10\%}$	$4138^{+10.1\%}_{-9.5\%}$	$3709^{+12.3\%}_{-8.8\%}$	$4060^{+11.1\%}_{-8.5\%}$
	2	$4322^{+4.2\%}_{-5.3\%}$	$4338^{+3.5\%}_{-4.8\%}$	$4424^{+1.9\%}_{-3.1\%}$	$4283^{+4.2\%}_{-5.0\%}$	$4394^{+2.4\%}_{-3.4\%}$
	3	$4439^{+0.51\%}_{-1.8\%}$	$4440^{+0.47\%}_{-1.6\%}$	$4448^{+0.26\%}_{-0.77\%}$	$4427^{+0.76\%}_{-2.0\%}$	$4444^{+0.35\%}_{-1.02\%}$

Table 1: Inclusive cross sections (in unit of fb) with the $m_t \rightarrow \infty$ approximation at both fixed order $N^k\text{LO}$ and resummation $N^k\text{LO}+N^k\text{LL}$ ($k = 0, 1, 2, 3$) in the center-of-mass energies $\sqrt{s} = 13, 14, 27, 100$ TeV. In the resummation, the results of four different resummation schemes have been shown. The quoted uncertainties are from the 7-point scale variations with the central scale $\mu_0 = \frac{m_{hh}}{2}$.

of $N^3\text{LO}+N^3\text{LL}$ are a factor 2 smaller than $N^3\text{LO}$ and almost a factor 4 smaller than $\text{NNLO}+\text{NNLL}$, reaching to the sub-percent level now. The cross sections in a wider energy interval from $\sqrt{s} = 7$ TeV to $\sqrt{s} = 100$ TeV are displayed in figure 3. In the left plot, we compare various resummation orders from $\text{LO}+\text{LL}$ to $N^3\text{LO}+N^3\text{LL}$. The error band of $N^k\text{LO}+N^k\text{LL}$, representing the 7-point scale uncertainties, resides completely in the band of the previous order when $k \geq 2$.¹⁹ Such an observation is analogous to the

¹⁹Without surprising, $\text{LO}+\text{LL}$ clearly underestimates the missing higher order by using the manner of

fixed order results [51, 52], with the exception that in the fixed order the N^3LO bands are outside the NLO counterparts. NLO+NLL increases LO+LL by 40% (50%) at 13 (100) TeV. NNLO+NNLL further enhances NLO+NLL by 6% and 8% respectively at these two energies. Furthermore, N^3LO+N^3LL improves the NNLO+NNLL cross sections by only 0.4% and 1% at $\sqrt{s} = 13$ and 100 TeV respectively. The right plot of figure 3 compares our best prediction N^3LO+N^3LL to the previous state-of-the-art results known in the literature (NNLO+NNLL and N^3LO). Because the (partial) higher orders beyond N^3LO have been included in the NNLO+NNLL resummation calculation, strictly speaking, N^3LO does not supersede NNLO+NNLL. In contrast, N^3LO+N^3LL is superior to both of them. This is why the comparison in the right plot would be also interesting. From the ratios in the lower panel, the difference in the central values of N^3LO and N^3LO+N^3LL is almost invisible, while the difference between NNLO+NNLL and N^3LO+N^3LL is visible but within a percent. However, the N^3LO error band is completely enclosed in the NNLO+NNLL band, and the N^3LO+N^3LL error band largely lies in the N^3LO band. This again points to the good asymptotic perturbative convergence.

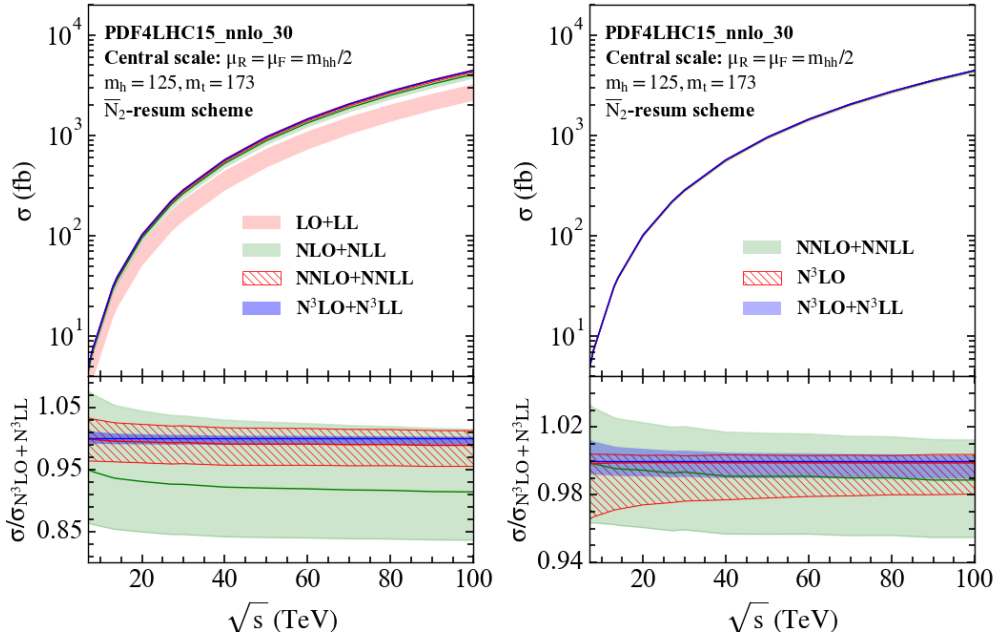


Figure 3: Inclusive cross sections with respect to the center of mass energies \sqrt{s} from LO+LL to N^3LO+N^3LL (left) and comparison study of the best result N^3LO+N^3LL against the previous best-known orders N^3LO and NNLO+NNLL (right). The error bands represent the 7-point scale uncertainties. In the lower panels, the ratios over the central value of N^3LO+N^3LL have been taken.

In the infinite top mass limit, the only exactly known differential cross sections at N^3LO is the invariant mass m_{hh} of the Higgs boson pair. While the other differential cross sections the scale variations.

are computed only at some approximation at this order [52] so far. The invariant mass distribution is a typical observable for demonstrating the impact of threshold resummation calculations. In the $m_t \rightarrow \infty$ approximation, we report the $\frac{d\sigma}{dm_{hh}}$ distributions in figure 4 at four distinct perturbative orders $N^k\text{LO}+N^k\text{LL}$ ($k = 0, 1, 2, 3$). The inclusion of higher order QCD radiative corrections dramatically stabilises the perturbative calculations of the invariant mass differential distributions. In particular, the shape of the distribution is almost unchanged from NLO+NLL to $N^3\text{LO}+N^3\text{LL}$ except the $m_{hh} \simeq 2m_h$ regime, while the scale uncertainties are significantly reduced as what have been observed in the inclusive cross section case. The results in four nominal energies in the figure show that the m_{hh} spectrum is harder from 13 TeV to 100 TeV because of the wider phase space with larger \sqrt{s} . From $k = 1$, the error bands of $N^{k+1}\text{LO}+N^{k+1}\text{LL}$ are completely enclosed within the previous-order $N^k\text{LO}+N^k\text{LL}$ uncertainty bands. We compare our best $N^3\text{LO}+N^3\text{LL}$ predictions to $N^3\text{LO}$ and NNLO+NNLL in figure 5. The message is again similar. The $N^3\text{LL}$ QCD corrections only marginally modify the shapes, and the $N^3\text{LO}+N^3\text{LL}$ results with sub-percent scale uncertainties are in both the $N^3\text{LO}$ and NNLO+NNLL error bands.

3.2 $N^3\text{LO}+N^3\text{LL}$ improved cross sections with full top-quark mass dependence

Unlike the single Higgs case, it is widely acknowledged that it would be crucial to include the finite top quark mass corrections in $gg \rightarrow hh$ for the realistic phenomenological applications. However, as aforementioned, the calculations in the full top quark mass dependence are very challenging, which are only best known at NLO+NLL [47]. In our paper, we will only use the NLO full m_t -dependent results (dubbed as “NLO $_{m_t}$ ” along the notation used in ref. [52]), which can be directly computed with the public code [48, 50]. In order to provide the best theoretical predictions, a common way people usually do is to combine the $m_t \rightarrow \infty$ results, which are precisely known, with the full m_t results. However, there are ambiguities on how to combine the two, featuring different underlying theoretical working assumptions. Several combination approaches have been studied in refs. [52, 80, 82]. In this paper, we will opt to improving the (differential) cross sections by multiplying the (differential) QCD K factors obtained in the $m_t \rightarrow \infty$ calculations, i.e.

$$\begin{aligned} d\sigma_{(N^k\text{LO}+N^k\text{LL})\otimes\text{NLO}_{m_t}} &\equiv d\sigma_{\text{NLO}_{m_t}} \frac{d\sigma_{N^k\text{LO}+N^k\text{LL}}}{d\sigma_{\text{NLO}}}, \\ d\sigma_{N^k\text{LO}\otimes\text{NLO}_{m_t}} &\equiv d\sigma_{\text{NLO}_{m_t}} \frac{d\sigma_{N^k\text{LO}}}{d\sigma_{\text{NLO}}}. \end{aligned} \quad (3.1)$$

Except the so-called “finite top (FT)” approximation [80, 82], which requires additional work that is beyond the scope of our paper, it is arguable that $(N^k\text{LO} + N^k\text{LL}) \otimes \text{NLO}_{m_t}$ (and $N^k\text{LO} \otimes \text{NLO}_{m_t}$) is the best combination among those presented in section 3 of ref. [52]. Therefore, we refrain ourselves from presenting our results in various combination schemes here, but instead just show $(N^k\text{LO} + N^k\text{LL}) \otimes \text{NLO}_{m_t}$ and $N^k\text{LO} \otimes \text{NLO}_{m_t}$. For NLO_{m_t} and $N^k\text{LO} \otimes \text{NLO}_{m_t}$, the results are essentially identical to ref. [52] except that we use 7-point scale variations in the current paper, while 9-point scale variations have been adopted in ref. [52]. The cross section in each scale choice is evaluated following

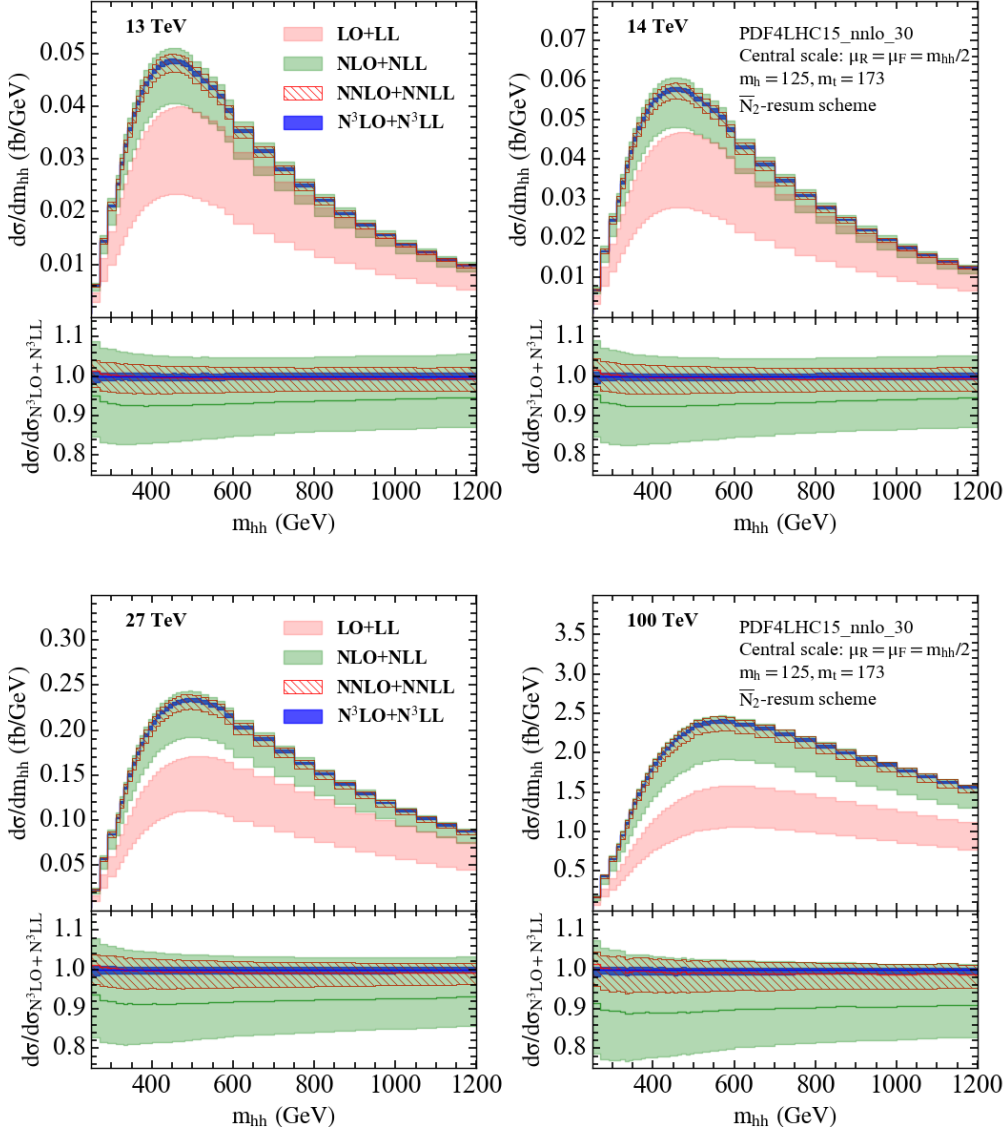


Figure 4: The invariant mass differential cross sections $\frac{d\sigma}{dm_{hh}}$ from LO+LL to $N^3\text{LO}+N^3\text{LL}$ at four different center-of-mass energies $\sqrt{s} = 13, 14, 27, 100$ TeV. The error bands represent the 7-point scale variations with the central scale $\mu_0 = \frac{m_{hh}}{2}$. The pink, green, red hatched and blue bands correspond to the LL+LO, NLO+NLL, NNLO+NNLL and $N^3\text{LO}+N^3\text{LL}$ predictions, respectively. The bottom panel shows the ratios to the $N^3\text{LO}+N^3\text{LL}$ distribution.

eq.(3.4) in ref. [52]. In other words, the relative scale errors in $(N^k\text{LO} + N^k\text{LL}) \otimes \text{NLO}_{m_t}$ and $N^k\text{LO} \otimes \text{NLO}_{m_t}$ are identical to those in $N^k\text{LO}+N^k\text{LL}$ and $N^k\text{LO}$ in the infinite top quark mass approximation. Though we have only taken into account NLO_{m_t} , we want to emphasize that the most advanced theoretical predictions can be easily obtained from our calculation even after the full m_t dependent NNLO result was available. In particular,

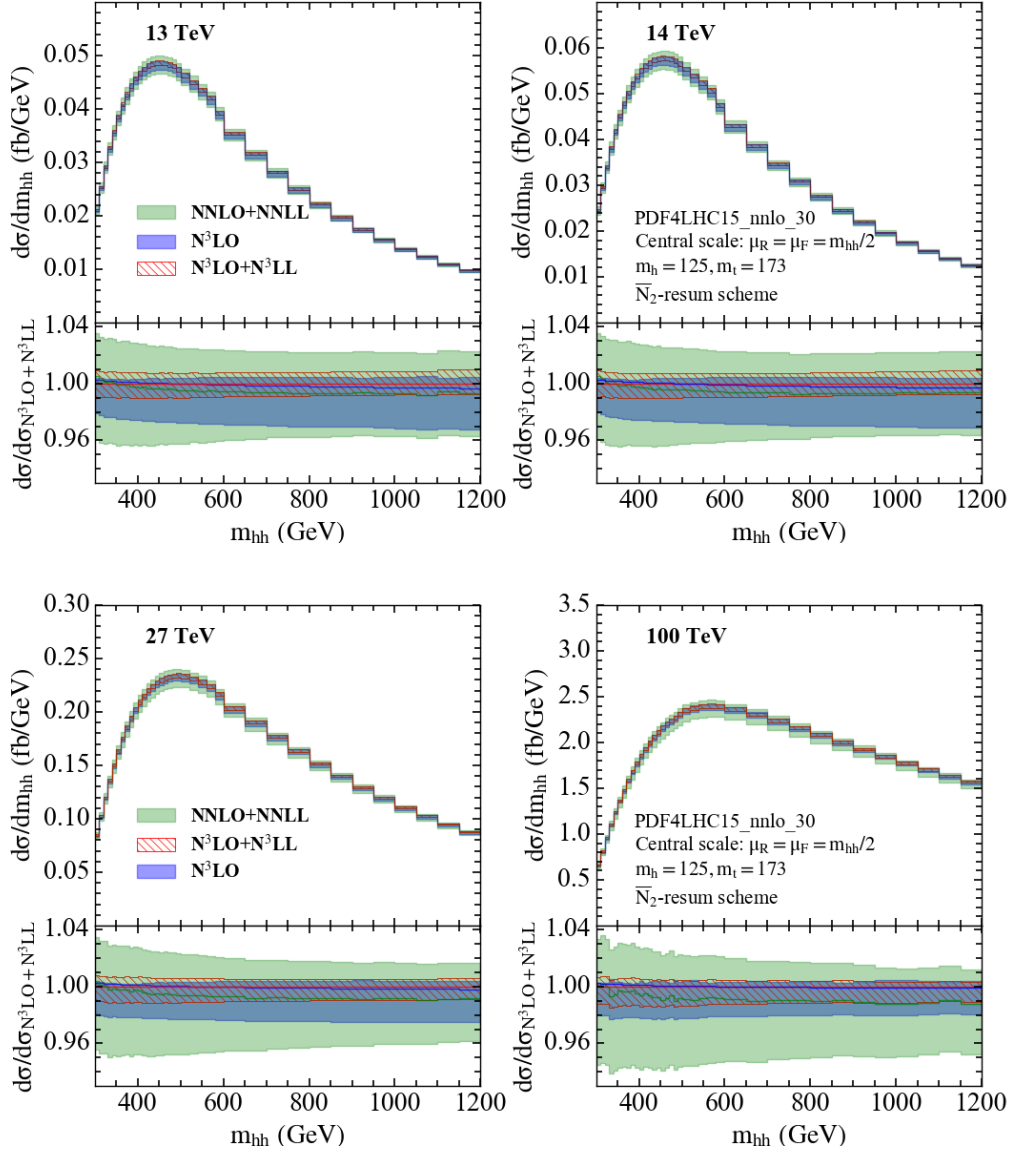


Figure 5: The comparisons of the invariant mass differential cross sections $\frac{d\sigma}{dm_{hh}}$ between N^3LO+N^3LL (blue) and N^3LO (red hatched) and $NNLO+NNLL$ (green) at four different center-of-mass energies $\sqrt{s} = 13, 14, 27, 100$ TeV. The error bands represent the 7-point scale variations with the central scale $\mu_0 = \frac{m_{hh}}{2}$. The bottom panel shows the ratios to the N^3LO+N^3LL distribution.

we suggest the current recommendation values proposed by the LHC Higgs Cross Section Working Group [22] can be improved with our results.

The total cross sections after including NLO_{m_t} are listed in table 2 at the 4 center-of-mass energies $\sqrt{s} = 13, 14, 27$ and 100 TeV. The results are obtained after applying eq.(3.1) to the total cross sections at $NNLO+NNLL$, N^3LO and N^3LO+N^3LL respec-

tively. In the table, we show the original NLO_{m_t} results without any further improvement too. The residual scale uncertainties range from 10% to 15%. There is another source of big theoretical uncertainties due to the top-quark mass scheme and the scale arbitrariness in the $\overline{\text{MS}}$ top quark mass that we have not yet quoted in the table, because such uncertainties are not expected to be reduced in our calculation with the infinite top quark mass approximation. In the inclusive total cross sections, these uncertainties are amount to +4%, -18% at the above four energies [42, 45]. In the following, we will only focus on the conventional renormalisation and factorisation scale uncertainties. In the $\overline{\text{N}}_2$ resummation scheme, $(\text{NNLO} + \text{NNLL}) \otimes \text{NLO}_{m_t}$ enhances the central values of the NLO_{m_t} cross sections by around 20%, while the scale uncertainties have been reduced to $\sim \pm 3\%$. Meanwhile, $\text{N}^3\text{LO} \otimes \text{NLO}_{m_t}$ increases the NLO_{m_t} cross sections by a similar amount, but reduces the relative scale uncertainties to -0.5% , $+2.5\%$, being very asymmetric and almost a factor 2 smaller than $(\text{NNLO} + \text{NNLL}) \otimes \text{NLO}_{m_t}$. Our most advanced predictions $(\text{N}^3\text{LO} + \text{N}^3\text{LL}) \otimes \text{NLO}_{m_t}$ shrink such uncertainties by another factor of two, reaching to the sub-percent level. Our best predictions for the di-Higgs cross sections are 33.47, 39.60, 151.9, 1335 fb at $\sqrt{s} = 13, 14, 27, 100$ TeV. We want to stress that though the central values of $(\text{NNLO} + \text{NNLL}) \otimes \text{NLO}_{m_t}$ are very close to $(\text{N}^3\text{LO} + \text{N}^3\text{LL}) \otimes \text{NLO}_{m_t}$, such a conclusion will alter if one chooses either N_1 or $\overline{\text{N}}_1$ resummation schemes.

\sqrt{s}	13 TeV	14 TeV	27 TeV	100 TeV
NLO_{m_t}	$27.56^{+13.9\%}_{-12.7\%}$	$32.64^{+13.5\%}_{-12.47\%}$	$126.1^{+11.5\%}_{-10.4\%}$	$1119^{+10.7\%}_{-9.9\%}$
$(\text{NNLO} + \text{NNLL}) \otimes \text{NLO}_{m_t}$	$33.33^{+3.0\%}_{-3.3\%}$	$39.42^{+3.0\%}_{-3.4\%}$	$150.8^{+2.7\%}_{-3.4\%}$	$1320^{+2.4\%}_{-3.4\%}$
$\text{N}^3\text{LO} \otimes \text{NLO}_{m_t}$	$33.43^{+0.50\%}_{-2.8\%}$	$39.56^{+0.50\%}_{-2.7\%}$	$151.7^{+0.46\%}_{-2.3\%}$	$1333^{+0.51\%}_{-1.8\%}$
$(\text{N}^3\text{LO} + \text{N}^3\text{LL}) \otimes \text{NLO}_{m_t}$	$33.47^{+0.88\%}_{-0.85\%}$	$39.60^{+0.85\%}_{-0.87\%}$	$151.9^{+0.63\%}_{-0.94\%}$	$1335^{+0.35\%}_{-1.0\%}$

Table 2: The inclusive total cross sections (in unit of fb) of Higgs pair production at $\sqrt{s} = 13, 14, 27, 100$ TeV after taking into account the NLO full top quark mass dependence. The quoted relative uncertainties are from the 7-point scale variations.

Figure 6 is our predictions for the invariant mass distributions after taking into account the NLO full top-quark mass dependence. Four theoretical bands in each plot are the NLO_{m_t} (grey bands), $(\text{NNLO} + \text{NNLL}) \otimes \text{NLO}_{m_t}$ (green bands), $\text{N}^3\text{LO} \otimes \text{NLO}_{m_t}$ (red hatched bands), and $(\text{N}^3\text{LO} + \text{N}^3\text{LL}) \otimes \text{NLO}_{m_t}$ (blue bands) results. In principle, the infinite top quark mass approximation works better in the lower m_{hh} regime. This is indeed indicated in figure 6 that the $m_t \rightarrow \infty$ improved bands are only in the NLO_{m_t} bands when $m_{hh} < 300$ GeV. Beyond 300 GeV, the K factors are almost constants around 1.2, which can be evidently seen in the lower panels. Due to the manner of our combination, the remaining messages are essentially similar as what have been discussed in the previous subsection.

Before closing this section, we assess the missing top quark mass uncertainties beyond NLO. This kind of uncertainty is stemming from the lack of full m_t -dependent calculations

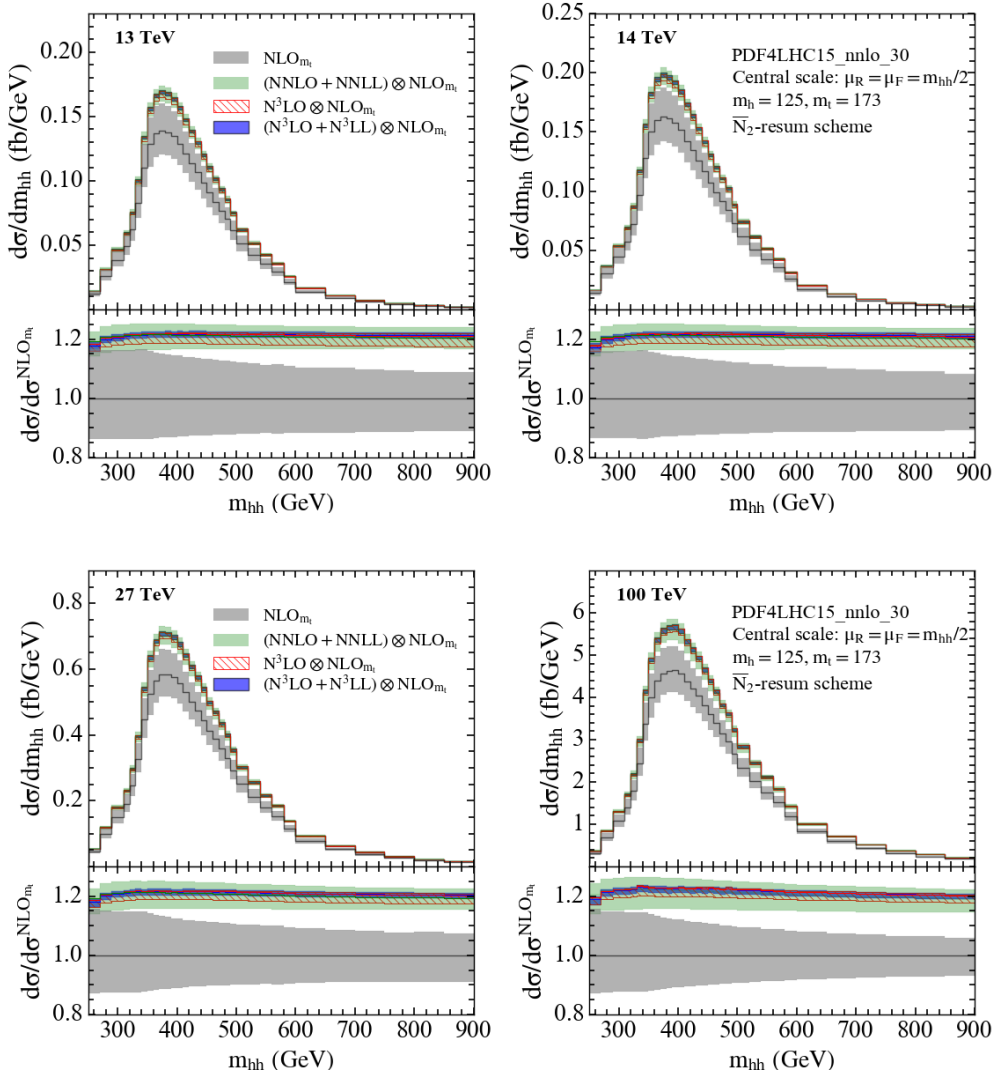


Figure 6: The invariant mass m_{hh} distributions with finite top quark mass corrections at four center-of-mass energies $\sqrt{s} = 13, 14, 27, 100$ TeV. The error bands are from the 7-point scale variations. The grey, green, red hatched and blue bands correspond to the NLO_{m_t} , $(\text{NNLO} + \text{NNLL}) \otimes \text{NLO}_{m_t}$, $\text{N}^3\text{LO} \otimes \text{NLO}_{m_t}$ and $(\text{N}^3\text{LO} + \text{N}^3\text{LL}) \otimes \text{NLO}_{m_t}$ predictions, respectively. The bottom panel shows the ratios to the NLO_{m_t} distribution.

at NNLO and beyond. Since we are working in the infinite top quark mass approximation, we do not expect the inclusion of higher order in α_s will improve such an uncertainty. In other words, the missing top quark mass uncertainty at $(\text{N}^3\text{LO} + \text{N}^3\text{LL}) \otimes \text{NLO}_{m_t}$ should be as large as those at $\text{NNLO} \otimes \text{NLO}_{m_t}$ and $\text{N}^3\text{LO} \otimes \text{NLO}_{m_t}$. The latter has been discussed in ref. [52] by comparing $\text{NNLO} \otimes \text{NLO}_{m_t}$ with respect to the so-called FT approximation at NNLO [82]. This missing top quark mass uncertainty is found to be around 5% at the LHC energies to 9% at 100 TeV. Our best predictions at $(\text{N}^3\text{LO} + \text{N}^3\text{LL}) \otimes \text{NLO}_{m_t}$ is envisaged to be further improved by combining with the NNLO FT approximation

calculations, which we leave it for the future work.

4 Summary

We have improved the (differential) cross section calculation of the Higgs boson pair production via gluon-gluon fusion with the threshold resummation up to N^3LL in the infinite top quark mass approximation. Such a resummation calculation has been consistently matched to the known N^3LO results. We first study the theoretical uncertainties at various perturbative orders due to the ambiguities in the resummation formalism. Though such resummation scheme uncertainties are in anyway sub-dominant at N^3LO+N^3LL , we argue that the N_2 and \bar{N}_2 schemes should give us the best predictions. With the \bar{N}_2 scheme, the residual renormalisation and factorisation scale uncertainties are less than one percent, which are a factor of 2 smaller than N^3LO and a factor of 4 smaller than $NNLO+NNLL$, while the central values are almost identical to N^3LO . This further consolidates the observation that the asymptotic convergence in the strong coupling constant α_s series has reached at the fourth order [51, 52]. Such a conclusion holds for both the inclusive total cross sections and the differential invariant mass m_{hh} distributions.

Our results have been finally combined with the full top quark mass dependent calculation at NLO QCD. Such combinations are essential for phenomenological applications. The new predictions of the di-Higgs hadroproduction cross sections have been reported after taking into account the finite top quark mass corrections.

Regarding the prospects for the future, it is clear that how to reduce the large top-quark mass scheme uncertainty remains an open question. In addition, the NNLO QCD and NLO electroweak calculations in the SM would be quite desirable, which are however quite technically challenging. The top-quark mass scheme uncertainty is expected to be reduced if the full NNLO QCD calculation in the SM was available. The minor percent level bottom-quark-loop contributions would turn out to be interesting too given the subpercent level scale uncertainty we have reached in this paper.

Acknowledgements

We thank L.-B. Chen, G. Das, H. T. Li, P. Mukherjee, V. Ravindran, and J. Wang for the collaboration at the initial stage of the project. We acknowledge the useful discussions with them at the different stages of this project. We are in particular grateful to H. T. Li for providing a grid of a two-loop amplitude and for checking the hard function against ref. [52]. This work is supported by the European Union’s Horizon 2020 research and innovation programme (grant agreement No.824093, STRONG-2020, EU Virtual Access “NLOAccess”), the ERC grant (grant agreement ID 101041109, “BOSON”), the French ANR (grant ANR-20-CE31-0015, “PrecisOnium”), and the CNRS IEA (grant No.205210, “GlueGraph”).

A The universal N³LL resummed coefficients

In this appendix, we provide the explicit expressions of the process-independent ingredients in the resummed partonic coefficient function $\Delta_{gg}^{\text{res}}(N, M^2, \mu_F^2)$ [eq. (2.47)] for the gluon-gluon induced colourless final states in QCD with $n_q = 5$. For the purpose of the discussions in subsection 2.4, we would like to split $\tilde{C}_{0,gg}$ into two pieces

$$\tilde{C}_{0,gg} = \tilde{C}_{0,gg,\gamma_E} + \tilde{C}_{00,gg,\zeta}, \quad (\text{A.1})$$

where the first piece $\tilde{C}_{0,gg,\gamma_E}$ is proportional to the Euler-Mascheroni constant γ_E and the second term solely depends on the Riemann zeta function which can be obtained by setting $\gamma_E = 0$ in $\tilde{C}_{0,gg}$. The first N -independent universal part has the following a_s series

$$2 \ln \mathcal{S}_{gg,\delta}^{\text{fin}} - 2 \ln \Gamma_{gg,\delta}^{\text{fin}} + \tilde{C}_{0,gg,\gamma_E} = \sum_{k=1} a_s^k G_{gg,0}^{(k)}. \quad (\text{A.2})$$

Up to three loops, we have

$$G_{gg,0}^{(1)} = -L_{fr} \frac{46}{3} + 6L_{qr}^2 - 18\zeta_2 + 24\gamma_E(\gamma_E + L_{fr} - L_{qr}), \quad (\text{A.3})$$

$$\begin{aligned} G_{gg,0}^{(2)} = & L_{fr}^2 \frac{529}{9} - L_{fr} \left(\frac{256}{3} + 216\zeta_3 \right) - L_{qr}^3 \frac{46}{3} + L_{qr}^2 \left(\frac{302}{3} - 36\zeta_2 \right) - L_{qr} \left(\frac{1864}{9} \right. \\ & \left. - 252\zeta_3 - 184\zeta_2 \right) + \frac{5644}{27} - \zeta_2 \frac{1057}{3} + 36\zeta_2^2 - \zeta_3 \frac{782}{3} + \gamma_E^3 \frac{368}{3} + \gamma_E^2 \left(\frac{1208}{3} - 184L_{qr} - 144\zeta_2 \right) \\ & \left. + \gamma_E \left[\frac{3728}{9} + \left(\frac{1208}{3} - 144\zeta_2 \right) (L_{fr} - L_{qr}) - 92(L_{fr}^2 - L_{qr}^2) - 504\zeta_3 \right], \quad (\text{A.4}) \right. \end{aligned}$$

$$\begin{aligned} G_{gg,0}^{(3)} = & L_{fr} \left(96\zeta_2 - 276\zeta_2^2 - 7248\zeta_3 + 864\zeta_2\zeta_3 + 4320\zeta_5 - \frac{20881}{27} \right) + L_{fr}^2 \left(1656\zeta_3 + \frac{2852}{3} \right) \\ & - L_{fr}^3 \frac{24334}{81} + L_{qr} \left(\zeta_2 \frac{78976}{9} - \zeta_2^2 \frac{8584}{5} + \zeta_3 \frac{122768}{9} - 1584\zeta_2\zeta_3 - 5184\zeta_5 - \frac{1472291}{243} \right) \\ & + L_{qr}^2 \left(\frac{73097}{27} - \frac{7856}{3}\zeta_2 + \zeta_2^2 \frac{2376}{5} - 2056\zeta_3 \right) - L_{qr}^3 \left(\frac{15980}{27} - 184\zeta_2 \right) + L_{qr}^4 \frac{529}{9} \\ & + \frac{26820931}{4374} - \zeta_2 \frac{935587}{81} + \zeta_2^2 \frac{107866}{45} + \zeta_2^3 \frac{304}{7} - \zeta_3 \frac{1416988}{81} + \zeta_2\zeta_3 \frac{31724}{3} \\ & + 3216\zeta_3^2 - \zeta_5 \frac{23816}{9} + \gamma_E^4 \frac{8464}{9} + \gamma_E^3 \left(\frac{127840}{27} - L_{qr} \frac{16928}{9} - 1472\zeta_2 \right) \\ & \left. + \gamma_E^2 \left[\frac{292388}{27} + L_{qr} \left(-\frac{63920}{9} + 2208\zeta_2 \right) + L_{qr}^2 \frac{4232}{3} - 4832\zeta_2 + \zeta_2^2 \frac{9504}{5} - 8224\zeta_3 \right] \right. \\ & + \gamma_E \left[L_{fr} \left(\frac{40300}{9} - 4832\zeta_2 + \zeta_2^2 \frac{9504}{5} - 496\zeta_3 \right) + (L_{qr}^2 - L_{fr}^2) \left(\frac{31960}{9} - 1104\zeta_2 \right) \right. \\ & + (L_{fr}^3 - L_{qr}^3) \frac{4232}{9} + L_{qr} \left(-\frac{292388}{27} + 4832\zeta_2 - \zeta_2^2 \frac{9504}{5} + 8224\zeta_3 \right) + \frac{2944582}{243} \\ & \left. - \zeta_2 \frac{30112}{9} - \zeta_2^2 \frac{4912}{5} - \zeta_3 \frac{177824}{9} + 3168\zeta_2\zeta_3 + 10368\zeta_5 \right], \quad (\text{A.5}) \end{aligned}$$

where we have defined $L_{qr} \equiv \ln \frac{M^2}{\mu_R^2}$ and $L_{fr} \equiv \ln \frac{\mu_F^2}{\mu_R^2}$. In the above equations, the γ_E terms are purely from $\tilde{C}_{0,gg,\gamma_E}$. Therefore, the expressions for $2 \ln \mathcal{S}_{gg,\delta}^{\text{fin}} - 2 \ln \Gamma_{gg,\delta}^{\text{fin}}$ can be obtained

directly by setting $\gamma_E = 0$. For $\tilde{C}_{0,gg,\zeta}$, we have the similar a_s series $\tilde{C}_{0,gg,\zeta} = \sum_{k=1} a_s^k \tilde{C}_{0,gg,\zeta}^{(k)}$ with the coefficients

$$\tilde{C}_{0,gg,\zeta}^{(1)} = 24\zeta_2, \quad (\text{A.6})$$

$$\tilde{C}_{0,gg,\zeta}^{(2)} = \zeta_2 \frac{1208}{3} - 184L_{qr}\zeta_2 - 144\zeta_2^2 + \zeta_3 \frac{736}{3}, \quad (\text{A.7})$$

$$\begin{aligned} \tilde{C}_{0,gg,\zeta}^{(3)} &= L_{qr} \left(-\zeta_2 \frac{63920}{9} + 2208\zeta_2^2 - \zeta_3 \frac{33856}{9} \right) + L_{qr}^2 \zeta_2 \frac{4232}{3} + \zeta_2 \frac{292388}{27} - \zeta_2^2 \frac{80944}{15} \\ &\quad + \zeta_2^3 \frac{9504}{5} + \zeta_3 \frac{255680}{27} - 11168\zeta_2\zeta_3. \end{aligned} \quad (\text{A.8})$$

The N -dependent coefficients as given in the exponent of eq. (2.47) are

$$g_{1,gg}(\omega) = \frac{72}{23} \frac{1}{\omega} \left[(1-\omega) \ln(1-\omega) + \omega \right], \quad (\text{A.9})$$

$$\begin{aligned} g_{2,gg}(\omega) &= \ln^2(1-\omega) \frac{6264}{12167} + \ln(1-\omega) \left(\frac{-29148}{12167} - \frac{72\gamma_E}{23} + \frac{36L_{qr}}{23} + \frac{648\zeta_2}{529} \right) \\ &\quad + \omega \left(\frac{-29148}{12167} + \frac{36L_{fr}}{23} + \frac{648\zeta_2}{529} \right), \end{aligned} \quad (\text{A.10})$$

$$\begin{aligned} g_{3,gg}(\omega) &= \frac{1}{(-1+\omega)} \left[\frac{-726624}{279841} \ln^2(1-\omega) + \ln(1-\omega) \left(\frac{151578}{12167} + \frac{8352\gamma_E}{529} - \frac{4176L_{qr}}{529} - \frac{75168\zeta_2}{12167} \right) \right. \\ &\quad + \omega^2 \left(\frac{-2965030}{279841} + \frac{604L_{fr}}{23} - 6L_{fr}^2 + \frac{212472\zeta_2}{12167} - \frac{216L_{fr}\zeta_2}{23} - \frac{21384\zeta_2^2}{2645} + \frac{1116\zeta_3}{529} \right) \\ &\quad + \omega \left(\frac{-531322}{36501} - \frac{19432\gamma_E}{529} - 24\gamma_E^2 - \frac{604L_{fr}}{23} + 6L_{fr}^2 + \frac{9716L_{qr}}{529} + 24\gamma_E L_{qr} - 6L_{qr}^2 \right. \\ &\quad \left. \left. - \frac{105126}{279841} \ln(1-\omega) - \frac{75168\zeta_2}{12167} + \frac{432\gamma_E\zeta_2}{23} + \frac{216L_{fr}\zeta_2}{23} - \frac{216L_{qr}\zeta_2}{23} + \frac{756\zeta_3}{23} \right) \right], \end{aligned} \quad (\text{A.11})$$

$$\begin{aligned}
g_{4,gg}(\omega) = & \frac{1}{(-1+\omega)^2} \left\{ \frac{-28096128}{6436343} \ln^3(1-\omega) + \ln^2(1-\omega) \left(\frac{12191136}{279841} + \frac{484416\gamma_E}{12167} \right. \right. \\
& - \frac{242208L_{qr}}{12167} - \frac{4359744\zeta_2}{279841} \left. \right) + \ln(1-\omega) \left(\frac{-519707665}{2518569} - \frac{140128\gamma_E}{529} - \frac{2784\gamma_E^2}{23} \right. \\
& + \frac{70064L_{qr}}{529} + \frac{2784\gamma_E L_{qr}}{23} - \frac{696L_{qr}^2}{23} + \frac{24646752\zeta_2}{279841} + \frac{50112\gamma_E\zeta_2}{529} - \frac{25056L_{qr}\zeta_2}{529} \\
& - \frac{2480544\zeta_2^2}{60835} + \frac{2852192\zeta_3}{12167} \left. \right) + \omega^2 \left[\frac{-3406003448}{22667121} - \frac{63148756\gamma_E}{109503} - \frac{1208\gamma_E^2}{3} \right. \\
& - \frac{368\gamma_E^3}{3} - \frac{40300L_{fr}}{69} + \frac{31960L_{fr}^2}{69} - \frac{184L_{fr}^3}{3} + \frac{31574378L_{qr}}{109503} + \frac{1208\gamma_E L_{qr}}{3} \\
& + 184\gamma_E^2 L_{qr} - \frac{302L_{qr}^2}{3} - 92\gamma_E L_{qr}^2 + \frac{46L_{qr}^3}{3} - \frac{203879104\zeta_2}{839523} + \frac{141648\gamma_E\zeta_2}{529} \\
& + 144\gamma_E^2\zeta_2 + \frac{14496L_{fr}\zeta_2}{23} - 144L_{fr}^2\zeta_2 - \frac{70824L_{qr}\zeta_2}{529} - 144\gamma_E L_{qr}\zeta_2 + 36L_{qr}^2\zeta_2 \\
& + \frac{26054472\zeta_2^2}{60835} - \frac{14256\gamma_E\zeta_2^2}{115} - \frac{28512L_{fr}\zeta_2^2}{115} + \frac{7128L_{qr}\zeta_2^2}{115} - \frac{3036528\zeta_2^3}{18515} \\
& + \frac{14431616\zeta_3}{36501} + \frac{12336\gamma_E\zeta_3}{23} + \frac{1488L_{fr}\zeta_3}{23} - \frac{6168L_{qr}\zeta_3}{23} - \frac{41256\zeta_2\zeta_3}{529} - \frac{34992\zeta_3^2}{529} \\
& + \ln(1-\omega) \left(\frac{-965392751}{57927087} + \frac{705728\zeta_3}{12167} \right) - \frac{98592\zeta_5}{529} \left. \right] + \omega^3 \left(\frac{-5557403702}{57927087} + \frac{20150L_{fr}}{69} \right. \\
& - \frac{15980L_{fr}^2}{69} + \frac{92L_{fr}^3}{3} + \frac{172965524\zeta_2}{839523} - \frac{7248L_{fr}\zeta_2}{23} + 72L_{fr}^2\zeta_2 - \frac{15243576\zeta_2^2}{60835} + \\
& \frac{14256L_{fr}\zeta_2^2}{115} + \frac{2024352\zeta_2^3}{18515} + \frac{3204880\zeta_3}{36501} - \frac{744L_{fr}\zeta_3}{23} - \frac{8928\zeta_2\zeta_3}{529} + \frac{23328\zeta_3^2}{529} \\
& - \frac{53504\zeta_5}{529} \left. \right) + \omega \left[\frac{13235995612}{22667121} + \frac{5463772\gamma_E}{4761} + \frac{2416\gamma_E^2}{3} + \frac{736\gamma_E^3}{3} + \frac{20150L_{fr}}{69} \right. \\
& - \frac{15980L_{fr}^2}{69} + \frac{92L_{fr}^3}{3} - \frac{2731886L_{qr}}{4761} - \frac{2416\gamma_E L_{qr}}{3} - 368\gamma_E^2 L_{qr} + \frac{604L_{qr}^2}{3} \\
& + 184\gamma_E L_{qr}^2 - \frac{92L_{qr}^3}{3} - \frac{109246096\zeta_2}{839523} - \frac{283296\gamma_E\zeta_2}{529} - 288\gamma_E^2\zeta_2 - \frac{7248L_{fr}\zeta_2}{23} \\
& + 72L_{fr}^2\zeta_2 + \frac{141648L_{qr}\zeta_2}{529} + 288\gamma_E L_{qr}\zeta_2 - 72L_{qr}^2\zeta_2 - \frac{6378216\zeta_2^2}{60835} + \frac{28512\gamma_E\zeta_2^2}{115} \\
& + \frac{14256L_{fr}\zeta_2^2}{115} - \frac{14256L_{qr}\zeta_2^2}{115} + \ln(1-\omega) \left(\frac{88719002}{2518569} - \frac{1411456\zeta_3}{12167} \right) - \frac{38477872\zeta_3}{36501} \\
& \left. - \frac{24672\gamma_E\zeta_3}{23} - \frac{744L_{fr}\zeta_3}{23} + \frac{12336L_{qr}\zeta_3}{23} + \frac{4752\zeta_2\zeta_3}{23} + \frac{15552\zeta_5}{23} \right] \left. \right\}. \quad (\text{A.12})
\end{aligned}$$

References

- [1] ATLAS collaboration, G. Aad et al.,
Observation of a new particle in the search for the Standard Model Higgs boson with the ATLAS detector at the LHC, *Phys. Lett. B* **716** (2012) 1–29, [[1207.7214](#)].

- [2] CMS collaboration, S. Chatrchyan et al.,
Observation of a New Boson at a Mass of 125 GeV with the CMS Experiment at the LHC,
[Phys. Lett. B](#) **716** (2012) 30–61, [[1207.7235](#)].
- [3] ATLAS collaboration,
A detailed map of Higgs boson interactions by the ATLAS experiment ten years after the discovery,
[Nature](#) **607** (2022) 52–59, [[2207.00092](#)].
- [4] CMS collaboration,
A portrait of the Higgs boson by the CMS experiment ten years after the discovery, [Nature](#)
607 (2022) 60–68, [[2207.00043](#)].
- [5] L.-B. Chen, H. T. Li, H.-S. Shao and J. Wang, Higgs boson pair production at N³LO QCD,
[PoS ICHEP2020](#) (2021) 084, [[2011.04265](#)].
- [6] G. P. Salam, L.-T. Wang and G. Zanderighi, The Higgs boson turns ten, [Nature](#) **607** (2022)
41–47, [[2207.00478](#)].
- [7] G. Isidori, G. Ridolfi and A. Strumia, On the metastability of the standard model vacuum,
[Nucl. Phys.](#) **B609** (2001) 387–409, [[hep-ph/0104016](#)].
- [8] G. Degrandi, S. Di Vita, J. Elias-Miro, J. R. Espinosa, G. F. Giudice, G. Isidori and
A. Strumia, Higgs mass and vacuum stability in the Standard Model at NNLO, [JHEP](#) **08**
(2012) 098, [[1205.6497](#)].
- [9] S. Alekhin, A. Djouadi and S. Moch,
The top quark and Higgs boson masses and the stability of the electroweak vacuum, [Phys.](#)
[Lett.](#) **B716** (2012) 214–219, [[1207.0980](#)].
- [10] V. Branchina and E. Messina, Stability, Higgs Boson Mass and New Physics, [Phys. Rev.](#)
[Lett.](#) **111** (2013) 241801, [[1307.5193](#)].
- [11] L. Di Luzio, G. Isidori and G. Ridolfi,
Stability of the electroweak ground state in the Standard Model and its extensions, [Phys.](#)
[Lett.](#) **B753** (2016) 150–160, [[1509.05028](#)].
- [12] M. Dine, R. G. Leigh, P. Y. Huet, A. D. Linde and D. A. Linde,
Towards the theory of the electroweak phase transition, [Phys. Rev.](#) **D46** (1992) 550–571,
[[hep-ph/9203203](#)].
- [13] K. Kajantie, M. Laine, K. Rummukainen and M. E. Shaposhnikov,
Is there a hot electroweak phase transition at $m_H \gtrsim m_W$?, [Phys. Rev. Lett.](#) **77** (1996)
2887–2890, [[hep-ph/9605288](#)].
- [14] F. Csikor, Z. Fodor and J. Heitger, Endpoint of the hot electroweak phase transition, [Phys.](#)
[Rev. Lett.](#) **82** (1999) 21–24, [[hep-ph/9809291](#)].
- [15] M. E. Shaposhnikov, Baryon Asymmetry of the Universe in Standard Electroweak Theory,
[Nucl. Phys. B](#) **287** (1987) 757–775.
- [16] E. Witten, Cosmic Separation of Phases, [Phys. Rev. D](#) **30** (1984) 272–285.
- [17] C. Hogan, Gravitational radiation from cosmological phase transitions, [Mon. Not. Roy.](#)
[Astron. Soc.](#) **218** (1986) 629–636.
- [18] D. Grasso and H. R. Rubinstein, Magnetic fields in the early universe, [Phys. Rept.](#) **348**
(2001) 163–266, [[astro-ph/0009061](#)].

- [19] LHC HIGGS CROSS SECTION WORKING GROUP collaboration, D. de Florian et al., Handbook of LHC Higgs Cross Sections: 4. Deciphering the Nature of the Higgs Sector, [1610.07922](#).
- [20] M. Cepeda et al., Report from Working Group 2: Higgs Physics at the HL-LHC and HE-LHC, [CERN Yellow Rep. Monogr.](#) **7** (2019) 221–584, [[1902.00134](#)].
- [21] R. Contino et al., Physics at a 100 TeV pp collider: Higgs and EW symmetry breaking studies, [1606.09408](#).
- [22] J. Alison et al., Higgs Boson Pair Production at Colliders: Status and Perspectives, in Double Higgs Production at Colliders Batavia, IL, USA, September 4, 2018-9, 2019 (B. Di Micco, M. Gouzevitch, J. Mazzitelli and C. Vernieri, eds.), 2019, [1910.00012](#), <https://lss.fnal.gov/archive/2019/conf/fermilab-conf-19-468-e-t.pdf>.
- [23] S. Borowka, C. Duhr, F. Maltoni, D. Pagani, A. Shivaji and X. Zhao, Probing the scalar potential via double Higgs boson production at hadron colliders, [JHEP](#) **04** (2019) 016, [[1811.12366](#)].
- [24] W. Bizon, U. Haisch and L. Rottoli, Constraints on the quartic Higgs self-coupling from double-Higgs production at future hadron colliders, [JHEP](#) **10** (2019) 267, [[1810.04665](#)].
- [25] P. Huang, A. J. Long and L.-T. Wang, Probing the Electroweak Phase Transition with Higgs Factories and Gravitational Waves, [Phys. Rev. D](#) **94** (2016) 075008, [[1608.06619](#)].
- [26] A. Falkowski and R. Rattazzi, Which EFT, [JHEP](#) **10** (2019) 255, [[1902.05936](#)].
- [27] S. Chang and M. A. Luty, The Higgs Trilinear Coupling and the Scale of New Physics, [1902.05556](#).
- [28] ATLAS collaboration, Constraining the Higgs boson self-coupling from single- and double-Higgs production with the ATLAS detector, [2211.01216](#).
- [29] S. Kanemura, S. Kiyoura, Y. Okada, E. Senaha and C. P. Yuan, New physics effect on the Higgs selfcoupling, [Phys. Lett. B](#) **558** (2003) 157–164, [[hep-ph/0211308](#)].
- [30] D. O’Connell, M. J. Ramsey-Musolf and M. B. Wise, Minimal Extension of the Standard Model Scalar Sector, [Phys. Rev. D](#) **75** (2007) 037701, [[hep-ph/0611014](#)].
- [31] G. Cacciapaglia, H. Cai, A. Carvalho, A. Deandrea, T. Flacke, B. Fuks, D. Majumder and H.-S. Shao, Probing vector-like quark models with Higgs-boson pair production, [JHEP](#) **07** (2017) 005, [[1703.10614](#)].
- [32] D. Jurčiukonis and L. Lavoura, The three- and four-Higgs couplings in the general two-Higgs-doublet model, [JHEP](#) **12** (2018) 004, [[1807.04244](#)].
- [33] G. Durieux, M. McCullough and E. Salvioni, Gegenbauer’s Twin, [JHEP](#) **05** (2022) 140, [[2202.01228](#)].
- [34] F. Maltoni, D. Pagani and X. Zhao, Constraining the Higgs self-couplings at e^+e^- colliders, [JHEP](#) **07** (2018) 087, [[1802.07616](#)].

- [35] J. de Blas et al., Higgs Boson Studies at Future Particle Colliders, [JHEP 01 \(2020\) 139](#), [[1905.03764](#)].
- [36] M. L. Mangano, G. Ortona and M. Selvaggi, Measuring the Higgs self-coupling via Higgs-pair production at a 100 TeV p-p collider, [Eur. Phys. J. C 80 \(2020\) 1030](#), [[2004.03505](#)].
- [37] S. Borowka, G. Heinrich, S. P. Jones, M. Kerner, J. Schlenk and T. Zirke, SecDec-3.0: numerical evaluation of multi-scale integrals beyond one loop, [Comput. Phys. Commun. 196 \(2015\) 470–491](#), [[1502.06595](#)].
- [38] Z. Li, J. Wang, Q.-S. Yan and X. Zhao, Efficient numerical evaluation of Feynman integrals, [Chin. Phys. C40 \(2016\) 033103](#), [[1508.02512](#)].
- [39] J. Dick, On the convergence rate of the component-by-component construction of good lattice rules, [Journal of Complexity 20 \(2004\) 493 – 522](#).
- [40] S. Borowka, N. Greiner, G. Heinrich, S. P. Jones, M. Kerner, J. Schlenk, U. Schubert and T. Zirke, Higgs Boson Pair Production in Gluon Fusion at Next-to-Leading Order with Full Top-Quark Mass Dependence, [Phys. Rev. Lett. 117 \(2016\) 012001](#), [[1604.06447](#)].
- [41] S. Borowka, N. Greiner, G. Heinrich, S. P. Jones, M. Kerner, J. Schlenk and T. Zirke, Full top quark mass dependence in Higgs boson pair production at NLO, [JHEP 10 \(2016\) 107](#), [[1608.04798](#)].
- [42] J. Baglio, F. Campanario, S. Glaus, M. Muehlleitner, M. Spira and J. Streicher, Gluon fusion into Higgs pairs at NLO QCD and the top mass scheme, [Eur. Phys. J. C79 \(2019\) 459](#), [[1811.05692](#)].
- [43] J. Davies, G. Heinrich, S. P. Jones, M. Kerner, G. Mishima, M. Steinhauser and D. Wellmann, Double Higgs boson production at NLO: combining the exact numerical result and high-energy expansion, [JHEP 11 \(2019\) 024](#), [[1907.06408](#)].
- [44] J. Baglio, F. Campanario, S. Glaus, M. Muehlleitner, J. Ronca and M. Spira, $gg \rightarrow HH$: Combined uncertainties, [Phys. Rev. D 103 \(2021\) 056002](#), [[2008.11626](#)].
- [45] J. Baglio, F. Campanario, S. Glaus, M. Muehlleitner, J. Ronca, M. Spira and J. Streicher, Higgs-Pair Production via Gluon Fusion at Hadron Colliders: NLO QCD Corrections, [JHEP 04 \(2020\) 181](#), [[2003.03227](#)].
- [46] G. Ferrera and J. Pires, Transverse-momentum resummation for Higgs boson pair production at the LHC with top-quark mass effects, [JHEP 02 \(2017\) 139](#), [[1609.01691](#)].
- [47] D. De Florian and J. Mazzitelli, Soft gluon resummation for Higgs boson pair production including finite M_t effects, [JHEP 08 \(2018\) 156](#), [[1807.03704](#)].
- [48] G. Heinrich, S. P. Jones, M. Kerner, G. Luisoni and E. Vryonidou, NLO predictions for Higgs boson pair production with full top quark mass dependence matched to parton shower, [JHEP 08 \(2017\) 088](#), [[1703.09252](#)].
- [49] S. Jones and S. Kuttimalai, Parton Shower and NLO-Matching uncertainties in Higgs Boson Pair Production, [JHEP 02 \(2018\) 176](#), [[1711.03319](#)].

- [50] G. Heinrich, S. P. Jones, M. Kerner, G. Luisoni and L. Scyboz,
Probing the trilinear Higgs boson coupling in di-Higgs production at NLO QCD including parton shower effect, [JHEP](#) **06** (2019) 066, [[1903.08137](#)].
- [51] L.-B. Chen, H. T. Li, H.-S. Shao and J. Wang,
Higgs boson pair production via gluon fusion at N³LO in QCD, [Phys. Lett. B](#) **803** (2020) 135292, [[1909.06808](#)].
- [52] L.-B. Chen, H. T. Li, H.-S. Shao and J. Wang,
The gluon-fusion production of Higgs boson pair: N³LO QCD corrections and top-quark mass effects, [JHEP](#) **03** (2020) 072, [[1912.13001](#)].
- [53] S. Dawson, S. Dittmaier and M. Spira,
Neutral Higgs boson pair production at hadron colliders: QCD corrections, [Phys. Rev. D](#) **58** (1998) 115012, [[hep-ph/9805244](#)].
- [54] D. de Florian and J. Mazzitelli, Two-loop virtual corrections to Higgs pair production, [Phys. Lett. B](#) **724** (2013) 306–309, [[1305.5206](#)].
- [55] D. de Florian and J. Mazzitelli,
Higgs Boson Pair Production at Next-to-Next-to-Leading Order in QCD, [Phys. Rev. Lett.](#) **111** (2013) 201801, [[1309.6594](#)].
- [56] J. Grigo, K. Melnikov and M. Steinhauser,
Virtual corrections to Higgs boson pair production in the large top quark mass limit, [Nucl. Phys. B](#) **888** (2014) 17–29, [[1408.2422](#)].
- [57] D. de Florian, M. Grazzini, C. Hanga, S. Kallweit, J. M. Lindert, P. Maierhöfer, J. Mazzitelli and D. Rathlev,
Differential Higgs Boson Pair Production at Next-to-Next-to-Leading Order in QCD, [JHEP](#) **09** (2016) 151, [[1606.09519](#)].
- [58] M. Spira, Effective Multi-Higgs Couplings to Gluons, [JHEP](#) **10** (2016) 026, [[1607.05548](#)].
- [59] M. Gerlach, F. Herren and M. Steinhauser,
Wilson coefficients for Higgs boson production and decoupling relations to $\mathcal{O}(\alpha_s^4)$, [JHEP](#) **11** (2018) 141, [[1809.06787](#)].
- [60] C. Anastasiou, C. Duhr, F. Dulat, F. Herzog and B. Mistlberger,
Higgs Boson Gluon-Fusion Production in QCD at Three Loops, [Phys. Rev. Lett.](#) **114** (2015) 212001, [[1503.06056](#)].
- [61] B. Mistlberger, Higgs boson production at hadron colliders at N³LO in QCD, [JHEP](#) **05** (2018) 028, [[1802.00833](#)].
- [62] F. Dulat, A. Lazopoulos and B. Mistlberger, iHixs 2 — Inclusive Higgs cross sections, [Comput. Phys. Commun.](#) **233** (2018) 243–260, [[1802.00827](#)].
- [63] S. Catani and M. Grazzini,
An NNLO subtraction formalism in hadron collisions and its application to Higgs boson production at the LHC, [Phys. Rev. Lett.](#) **98** (2007) 222002, [[hep-ph/0703012](#)].
- [64] P. Banerjee, S. Borowka, P. K. Dhani, T. Gehrmann and V. Ravindran,
Two-loop massless QCD corrections to the $g + g \rightarrow H + H$ four-point amplitude, [JHEP](#) **11** (2018) 130, [[1809.05388](#)].
- [65] T. Gehrmann, T. Lubbert and L. L. Yang,

- Transverse parton distribution functions at next-to-next-to-leading order: the quark-to-quark case, [Phys. Rev. Lett.](#) **109** (2012) 242003, [[1209.0682](#)].
- [66] T. Gehrmann, T. Luebbert and L. L. Yang, [Calculation of the transverse parton distribution functions at next-to-next-to-leading order](#), [JHEP](#) **06** (2014) 155, [[1403.6451](#)].
- [67] M. G. Echevarria, I. Scimemi and A. Vladimirov, [Unpolarized Transverse Momentum Dependent Parton Distribution and Fragmentation Functions at next-to-next-to-leading order](#), [JHEP](#) **09** (2016) 004, [[1604.07869](#)].
- [68] M.-X. Luo, T.-Z. Yang, H. X. Zhu and Y. J. Zhu, [Transverse Parton Distribution and Fragmentation Functions at NNLO: the Gluon Case](#), [JHEP](#) **01** (2020) 040, [[1909.13820](#)].
- [69] M.-X. Luo, X. Wang, X. Xu, L. L. Yang, T.-Z. Yang and H. X. Zhu, [Transverse Parton Distribution and Fragmentation Functions at NNLO: the Quark Case](#), [JHEP](#) **10** (2019) 083, [[1908.03831](#)].
- [70] Y. Li and H. X. Zhu, [Bootstrapping Rapidity Anomalous Dimensions for Transverse-Momentum Resummation](#), [Phys. Rev. Lett.](#) **118** (2017) 022004, [[1604.01404](#)].
- [71] J. Alwall, R. Frederix, S. Frixione, V. Hirschi, F. Maltoni, O. Mattelaer, H. S. Shao, T. Stelzer, P. Torrielli and M. Zaro, [The automated computation of tree-level and next-to-leading order differential cross sections, and their matching to NLL resummation](#), [JHEP](#) **07** (2014) 079, [[1405.0301](#)].
- [72] R. Frederix, S. Frixione, V. Hirschi, D. Pagani, H. S. Shao and M. Zaro, [The automation of next-to-leading order electroweak calculations](#), [JHEP](#) **07** (2018) 185, [[1804.10017](#)].
- [73] D. de Florian and J. Mazzitelli, [Higgs pair production at next-to-next-to-leading logarithmic accuracy at the LHC](#), [JHEP](#) **09** (2015) 053, [[1505.07122](#)].
- [74] D. Y. Shao, C. S. Li, H. T. Li and J. Wang, [Threshold resummation effects in Higgs boson pair production at the LHC](#), [JHEP](#) **07** (2013) 169, [[1301.1245](#)].
- [75] J. Grigo, J. Hoff, K. Melnikov and M. Steinhauser, [On the Higgs boson pair production at the LHC](#), [Nucl. Phys. B](#) **875** (2013) 1–17, [[1305.7340](#)].
- [76] J. Grigo, J. Hoff and M. Steinhauser, [Higgs boson pair production: top quark mass effects at NLO and NNLO](#), [Nucl. Phys. B](#) **900** (2015) 412–430, [[1508.00909](#)].
- [77] G. Degrossi, P. P. Giardino and R. Gröber, [On the two-loop virtual QCD corrections to Higgs boson pair production in the Standard Model](#), [Eur. Phys. J. C](#) **76** (2016) 411, [[1603.00385](#)].
- [78] J. Davies, F. Herren, G. Mishima and M. Steinhauser, [Real-virtual corrections to Higgs boson pair production at NNLO: three closed top quark loops](#), [JHEP](#) **05** (2019) 157, [[1904.11998](#)].

- [79] J. Davies, F. Herren, G. Mishima and M. Steinhauser,
Real corrections to Higgs boson pair production at NNLO in the large top quark mass limit,
[JHEP](#) **01** (2022) 049, [[2110.03697](#)].
- [80] F. Maltoni, E. Vryonidou and M. Zaro,
Top-quark mass effects in double and triple Higgs production in gluon-gluon fusion at NLO,
[JHEP](#) **11** (2014) 079, [[1408.6542](#)].
- [81] R. Frederix, S. Frixione, V. Hirschi, F. Maltoni, O. Mattelaer, P. Torrielli, E. Vryonidou
and M. Zaro, Higgs pair production at the LHC with NLO and parton-shower effects,
[Phys. Lett. B](#) **732** (2014) 142–149, [[1401.7340](#)].
- [82] M. Grazzini, G. Heinrich, S. Jones, S. Kallweit, M. Kerner, J. M. Lindert and J. Mazzitelli,
Higgs boson pair production at NNLO with top quark mass effects, [JHEP](#) **05** (2018) 059,
[[1803.02463](#)].
- [83] J. Davies, G. Mishima, M. Steinhauser and D. Wellmann,
Double-Higgs boson production in the high-energy limit: planar master integrals, [JHEP](#) **03**
(2018) 048, [[1801.09696](#)].
- [84] J. Davies, G. Mishima, M. Steinhauser and D. Wellmann,
Double Higgs boson production at NLO in the high-energy limit: complete analytic results,
[JHEP](#) **01** (2019) 176, [[1811.05489](#)].
- [85] R. Bonciani, G. Degrassi, P. P. Giardino and R. Gröber,
Analytical Method for Next-to-Leading-Order QCD Corrections to Double-Higgs Production,
[Phys. Rev. Lett.](#) **121** (2018) 162003, [[1806.11564](#)].
- [86] X. Xu and L. L. Yang,
Towards a new approximation for pair-production and associated-production of the Higgs boson,
[JHEP](#) **01** (2019) 211, [[1810.12002](#)].
- [87] L. Bellafronte, G. Degrassi, P. P. Giardino, R. Gröber and M. Vitti,
Gluon fusion production at NLO: merging the transverse momentum and the high-energy expansions,
[JHEP](#) **07** (2022) 069, [[2202.12157](#)].
- [88] J. Davies, G. Mishima, K. Schönwald, M. Steinhauser and H. Zhang,
Higgs boson contribution to the leading two-loop Yukawa corrections to $gg \rightarrow HH$,
[2207.02587](#).
- [89] M. Mühlleitner, J. Schlenk and M. Spira,
Top-Yukawa-induced Corrections to Higgs Pair Production, [2207.02524](#).
- [90] S. Catani, The Singular behavior of QCD amplitudes at two loop order, [Phys. Lett.](#) **B427**
(1998) 161–171, [[hep-ph/9802439](#)].
- [91] G. F. Sterman and M. E. Tejeda-Yeomans, Multiloop amplitudes and resummation, [Phys.](#)
[Lett.](#) **B552** (2003) 48–56, [[hep-ph/0210130](#)].
- [92] V. Ravindran, J. Smith and W. L. van Neerven,
Two-loop corrections to Higgs boson production, [Nucl. Phys.](#) **B704** (2005) 332–348,
[[hep-ph/0408315](#)].
- [93] S. Moch, J. A. M. Vermaseren and A. Vogt,
Three-loop results for quark and gluon form-factors, [Phys. Lett.](#) **B625** (2005) 245–252,
[[hep-ph/0508055](#)].

- [94] S. M. Aybat, L. J. Dixon and G. F. Sterman,
The Two-loop anomalous dimension matrix for soft gluon exchange, [Phys. Rev. Lett.](#) **97** (2006) 072001, [[hep-ph/0606254](#)].
- [95] S. M. Aybat, L. J. Dixon and G. F. Sterman,
The Two-loop soft anomalous dimension matrix and resummation at next-to-next-to leading pole, [Phys. Rev.](#) **D74** (2006) 074004, [[hep-ph/0607309](#)].
- [96] T. Becher and M. Neubert,
Infrared singularities of scattering amplitudes in perturbative QCD, [Phys. Rev. Lett.](#) **102** (2009) 162001, [[0901.0722](#)].
- [97] E. Gardi and L. Magnea,
Factorization constraints for soft anomalous dimensions in QCD scattering amplitudes, [JHEP](#) **03** (2009) 079, [[0901.1091](#)].
- [98] O. Almelid, C. Duhr and E. Gardi,
Three-loop corrections to the soft anomalous dimension in multileg scattering, [Phys. Rev. Lett.](#) **117** (2016) 172002, [[1507.00047](#)].
- [99] O. Almelid, C. Duhr, E. Gardi, A. McLeod and C. D. White,
Bootstrapping the QCD soft anomalous dimension, [JHEP](#) **09** (2017) 073, [[1706.10162](#)].
- [100] S. Moch, J. A. M. Vermaseren and A. Vogt,
The Three loop splitting functions in QCD: The Nonsinglet case, [Nucl. Phys.](#) **B688** (2004) 101–134, [[hep-ph/0403192](#)].
- [101] A. Vogt, S. Moch and J. A. M. Vermaseren,
The Three-loop splitting functions in QCD: The Singlet case, [Nucl. Phys.](#) **B691** (2004) 129–181, [[hep-ph/0404111](#)].
- [102] J. Blümlein, P. Marquard, C. Schneider and K. Schönwald,
The three-loop unpolarized and polarized non-singlet anomalous dimensions from off shell operator matrix elements, [Nucl. Phys. B](#) **971** (2021) 115542, [[2107.06267](#)].
- [103] J. M. Henn, G. P. Korchemsky and B. Mistlberger,
The full four-loop cusp anomalous dimension in $\mathcal{N} = 4$ super Yang-Mills and QCD, [JHEP](#) **04** (2020) 018, [[1911.10174](#)].
- [104] A. von Manteuffel, E. Panzer and R. M. Schabinger,
Cusp and collinear anomalous dimensions in four-loop QCD from form factors, [Phys. Rev. Lett.](#) **124** (2020) 162001, [[2002.04617](#)].
- [105] G. Das, S.-O. Moch and A. Vogt,
Soft corrections to inclusive deep-inelastic scattering at four loops and beyond, [JHEP](#) **03** (2020) 116, [[1912.12920](#)].
- [106] G. Das, S. Moch and A. Vogt,
Approximate four-loop QCD corrections to the Higgs-boson production cross section, [Phys. Lett. B](#) **807** (2020) 135546, [[2004.00563](#)].
- [107] V. Ravindran, On Sudakov and soft resummations in QCD, [Nucl. Phys.](#) **B746** (2006) 58–76, [[hep-ph/0512249](#)].
- [108] A. H. Mueller, On the Asymptotic Behavior of the Sudakov Form-factor, [Phys. Rev.](#) **D20** (1979) 2037.

- [109] J. C. Collins, Algorithm to Compute Corrections to the Sudakov Form-factor, [Phys. Rev. D22 \(1980\) 1478](#).
- [110] A. Sen, Asymptotic Behavior of the Sudakov Form-Factor in QCD, [Phys. Rev. D24 \(1981\) 3281](#).
- [111] V. Ravindran, Higher-order threshold effects to inclusive processes in QCD, [Nucl. Phys. B752 \(2006\) 173–196](#), [[hep-ph/0603041](#)].
- [112] S. Moch, B. Ruijl, T. Ueda, J. M. Vermaseren and A. Vogt, On quartic colour factors in splitting functions and the gluon cusp anomalous dimension, [Phys. Lett. B 782 \(2018\) 627–632](#), [[1805.09638](#)].
- [113] A. Chakraborty, T. Huber, R. N. Lee, A. von Manteuffel, R. M. Schabinger, A. V. Smirnov, V. A. Smirnov and M. Steinhauser, The $Hb\bar{b}$ vertex at four loops and hard matching coefficients in SCET for various currents, [2204.02422](#).
- [114] T. Ahmed, A. H. Ajjath, G. Das, P. Mukherjee, V. Ravindran and S. Tiwari, Soft-virtual correction and threshold resummation for n -colorless particles to fourth order in QCD: Part I, [2010.02979](#).
- [115] Y. Li, A. von Manteuffel, R. M. Schabinger and H. X. Zhu, N³LO Higgs boson and Drell-Yan production at threshold: The one-loop two-emission contribution, [Phys. Rev. D90 \(2014\) 053006](#), [[1404.5839](#)].
- [116] S. Catani, L. Cieri, D. de Florian, G. Ferrera and M. Grazzini, Threshold resummation at N³LL accuracy and soft-virtual cross sections at N³LO, [Nucl. Phys. B888 \(2014\) 75–91](#), [[1405.4827](#)].
- [117] G. F. Sterman, Summation of Large Corrections to Short Distance Hadronic Cross-Sections, [Nucl. Phys. B 281 \(1987\) 310–364](#).
- [118] S. Catani and L. Trentadue, Resummation of the QCD Perturbative Series for Hard Processes, [Nucl. Phys. B 327 \(1989\) 323–352](#).
- [119] A. H. Ajjath, G. Das, M. C. Kumar, P. Mukherjee, V. Ravindran and K. Samanta, Resummed Drell-Yan cross-section at N³LL, [JHEP 10 \(2020\) 153](#), [[2001.11377](#)].
- [120] A. H. Ajjath, A. Chakraborty, G. Das, P. Mukherjee and V. Ravindran, Resummed prediction for Higgs boson production through $b\bar{b}$ annihilation at N³LL, [JHEP 11 \(2019\) 006](#), [[1905.03771](#)].
- [121] S. Moch and A. Vogt, Higher-order soft corrections to lepton pair and Higgs boson production, [Phys. Lett. B 631 \(2005\) 48–57](#), [[hep-ph/0508265](#)].
- [122] R. N. Lee, A. von Manteuffel, R. M. Schabinger, A. V. Smirnov, V. A. Smirnov and M. Steinhauser, Quark and Gluon Form Factors in Four-Loop QCD, [Phys. Rev. Lett. 128 \(2022\) 212002](#), [[2202.04660](#)].
- [123] C. Duhr and F. Dulat, PolyLogTools — polylogs for the masses, [JHEP 08 \(2019\) 135](#), [[1904.07279](#)].
- [124] M. Bonvini, S. Marzani, C. Muselli and L. Rottoli,

- On the Higgs cross section at $N^3\text{LO}+N^3\text{LL}$ and its uncertainty, [JHEP 08 \(2016\) 105](#), [[1603.08000](#)].
- [125] J. Butterworth et al., [PDF4LHC recommendations for LHC Run II](#), [J. Phys. G 43 \(2016\) 023001](#), [[1510.03865](#)].
- [126] S. Dulat, T.-J. Hou, J. Gao, M. Guzzi, J. Huston, P. Nadolsky, J. Pumplin, C. Schmidt, D. Stump and C. P. Yuan, [New parton distribution functions from a global analysis of quantum chromodynamics](#), [Phys. Rev. D 93 \(2016\) 033006](#), [[1506.07443](#)].
- [127] L. A. Harland-Lang, A. D. Martin, P. Motylinski and R. S. Thorne, [Parton distributions in the LHC era: MMHT 2014 PDFs](#), [Eur. Phys. J. C 75 \(2015\) 204](#), [[1412.3989](#)].
- [128] NNPDF collaboration, R. D. Ball et al., [Parton distributions for the LHC Run II](#), [JHEP 04 \(2015\) 040](#), [[1410.8849](#)].
- [129] A. Buckley, J. Ferrando, S. Lloyd, K. Nordström, B. Page, M. Rüfenacht, M. Schönherr and G. Watt, [LHAPDF6: parton density access in the LHC precision era](#), [Eur. Phys. J. C 75 \(2015\) 132](#), [[1412.7420](#)].